THE JOURNAL OF BIOLOGICAL CHEMISTRY VOL. 289, NO. 43, pp. 29801–29816, October 24, 2014
Published in the U.S.A.

Essential Role of the Zinc Finger Transcription Factor Casz1 for Mammalian Cardiac Morphogenesis and Development*[S]

Received for publication, April 5, 2014, and in revised form, September 2, 2014 Published, JBC Papers in Press, September 4, 2014, DOI 10.1074/jbc.M114.570416

Zhihui Liu[‡1], **Wenling Li**[§], **Xuefei Ma**[¶], **Nancy Ding**[‡], **Francesco Spallotta**[‖], **Eileen Southon**[**], **Lino Tessarollo**[**], **Carlo Gaetano**[‖2], **Yoh-suke Mukouyama**[§], **and Carol J. Thiele**[‡3]

From the [‡]*Pediatric Oncology Branch and the* [**]*Mouse Cancer Genetics Program, Neural Development Section, National Cancer Institute, Bethesda, Maryland 20892, the Laboratories of* [§]*Stem Cell and Neuro-vascular Biology and the* [¶]*Molecular Cardiology, NHLBI, National Institutes of Health, Bethesda, Maryland 20892, and the* [‖]*Division of Cardiovascular Epigenetics, Department of Cardiology, Goethe University, Frankfurt am Main 60596, Germany*

Background: The *CASZ1* (castor zinc finger 1) gene localizes to chromosome 1p36, and 1p36 deletion syndrome is related to congenital heart disease (CHD).
Results: *Casz1* knock-out mice exhibited abnormal heart development and phenocopies aspects of 1p36 deletion syndrome related CHD.
Conclusion: *CASZ1* is critical for mammalian heart development.
Significance: *CASZ1* may be a novel CHD gene, and this finding opens new avenues for human heart disease diagnosis and treatment.

Chromosome 1p36 deletion syndrome is one of the most common terminal deletions observed in humans and is related to congenital heart disease (CHD). However, the 1p36 genes that contribute to heart disease have not been clearly delineated. Human *CASZ1* gene localizes to 1p36 and encodes a zinc finger transcription factor. *Casz1* is required for *Xenopus* heart ventral midline progenitor cell differentiation. Whether *Casz1* plays a role during mammalian heart development is unknown. Our aim is to determine 1p36 gene *CASZ1* function at regulating heart development in mammals. We generated a *Casz1* knock-out mouse using *Casz1*-trapped embryonic stem cells. *Casz1* deletion in mice resulted in abnormal heart development including hypoplasia of myocardium, ventricular septal defect, and disorganized morphology. Hypoplasia of myocardium was caused by decreased cardiomyocyte proliferation. Comparative genome-wide RNA transcriptome analysis of *Casz1* depleted embryonic hearts identifies abnormal expression of genes that are critical for muscular system development and function, such as muscle contraction genes *TNNI2*, *TNNT1*, and *CKM*; contractile fiber gene *ACTA1*; and cardiac arrhythmia associated ion channel coding genes *ABCC9* and *CACNA1D*. The transcriptional regulation of some of these genes by *Casz1* was also found in cellular models. Our results showed that loss of *Casz1* during mouse development led to heart defect including cardiac noncompaction and ventricular septal defect, which phenocopies 1p36 deletion syndrome related CHD. This suggests that *CASZ1* is a novel 1p36 CHD gene and that the abnormal expression of cardiac morphogenesis and contraction genes induced by loss of *Casz1* contributes to the heart defect.

* This work was supported, in whole or in part, by the Intramural Research Program of the National Institutes of Health, the National Cancer Institute, and the Center for Cancer Research.
[S] This article contains supplemental Table S1.

[1] To whom correspondence may be addressed: 9000 Rockville Pike, Bldg. 10, Rm. 1W-3940, MSC-1105, Bethesda, MD 20892-1105. Tel.: 301-496-2321; Fax: 301-451-7052; E-mail: liuzhihu@mail.nih.gov.

[2] Supported by the LOEWE-CGT Centre of Excellence, Wolfgang Geothe University, and by Deutsche Forschungsgemeinschaft Program SFB834, "Endothelial Signaling and Vascular Repair," Project B11 (to C. G.).

[3] To whom correspondence may be addressed: 9000 Rockville Pike, Bldg. 10, Rm. 1W-3940, MSC-1105, Bethesda, MD 20892-1105. Tel.: 301-496-1543; Fax: 301-451-7052; E-mail: thielec@mail.nih.gov.

Congenital heart disease (CHD)[4] is the most common type of birth defect, affecting over 1% of all live births and accounting for one-third of all major congenital anomalies (1, 2). A heart developmental program is induced by developmentally regulated signal transduction molecules and mediated by tissue-specific transcription factors. These transcription factors repress lineage inappropriate genes and activate cardiac-specific genes such as those responsible for cardiac morphogenesis and contractility. Disruption of this process affects heart development and function (3–7). CHD is associated with chromosome anomalies such as Down syndrome (trisomy 21), deletion 1p36 syndrome, deletion 4p syndrome, and deletion 22q11 spectrum (2). Many of the genetic mutations associated with CHD encode transcription factors such as *GATA4*, *GATA6*, *TBX-5*, *TBX20*, *HAND1*, *HAND2*, *MYOCD*, and *NKX2.5* (2, 7). However, the underlying genetic basis of most forms of CHD remains unclear, necessitating further investigation into the genetic basis of CHD.

Human *CASZ1* is a 1p36 gene encodes a zinc finger transcription factor. *Casz1* was first described as a neural fate determination gene in *Drosophila* (8, 9). An *in situ* hybridization analysis of *Casz1* showing high levels of expression in the heart of developing mouse embryos was the first study to implicate *Casz1* in heart development (10). Our studies confirmed the relatively high levels of Casz1 in murine heart and showed ele-

[4] The abbreviations used are: CHD, congenital heart disease; E*n*, embryonic day *n*; H&E, hematoxylin and eosin; TUNEL, terminal deoxynucleotidyl-transferase-mediated dUTP nick end labeling; IPA, ingenuity pathway analysis; qRT-PCR, quantitative real time PCR; GSEA, gene set enrich analysis.

TABLE 1
Genotyping PCR primers

Primer name	Primer sequence
mCasz1WT-1869_s (cDNA)	CAGGATGTGATCCGACATTACAA
mCasz1–2102_a (cDNA)	GTTGATGAGCTGGGTGTTCTTCT
mCasz1_geo2_a (cDNA)	ATTCAGGCTGCGCAACTGTTGGG
mCasz1WT_s (genomic DNA)	AGCCAAAGGTATGTGGGGTCTAA
mCasz1WT_a (genomic DNA)	GCAGTGGAAGTGTGTGGTCTTCT
mCasz1Trap_a (genomic DNA)	TAAAGTGACCCTCCCAACAGCTT

vated CASZ1 levels in human heart (11, 12). Our studies also mapped *CASZ1* to the region of chromosome 1p36 loss of heterozygosity in neuroblastoma tumors and elucidated its function as a mammalian regulator of differentiation with tumor suppressor functions (11–15). Furthermore, a 1p36 deletion syndrome is associated with CHD, including noncompaction cardiomyopathy and ventricular septal defect (2, 16). The first functional evidence implicating *casz1* in heart development were studies in *Xenopus*, which indicated that *casz1* was required for heart ventral midline progenitor cell differentiation and vascular morphogenesis (17, 18). However, in mammals, the role *Casz1* plays during heart development is unknown.

Here we report that *Casz1* is critical for murine heart development. We find that *Casz1* deletion leads to abnormal cardiac gene expression and causes reduced cardiomyocyte proliferation, a ventricular septal defect and defective cardiac morphogenesis that ultimately led to heart failure and embryonic lethality. Our results demonstrate that *Casz1* is required for normal mammalian heart development and function.

MATERIALS AND METHODS

The Generation of Casz1$^{\beta geo/\beta geo}$ Mice—The 129 OLA *Casz1* trapped murine embryonic stem cells (Sanger CJ0565) were used to establish *Casz1* knock-out mouse. The *Casz1* gene trap inserted a βgeo reporter after *Casz1* exon 9 and was sequence verified. The embryonic stem cells were injected into C57BL6 blastocysts, and the chimeras were bred to C57BL6 wild type to generate mixed 129/C57BL6 mice as described previously (19). The characterization of *Casz1* mutant mice was performed by PCR using genomic DNA as template or reverse transcriptase PCR using cDNA as template. The primer sequences were listed in Table 1. All animals and procedures for mouse experiments were approved by the National Cancer Institute Animal Care and Use Committee.

X-Gal Staining—Embryos were fixed with 4% paraformaldehyde/PBS at 4 °C for 5 min. X-gal staining was performed as reported (20). In brief, the embryos were incubated with 1 mg/ml X-gal solution at 37 °C overnight. Postfixation with 4% paraformaldehyde/PBS was performed at room temperature for 25 min, and the embryos were sunk in 15% sucrose/PBS at 4 °C overnight. For sectioning, the embryos were embedded in gelatin and frozen dissected at 8-μm thickness, and then the slides were degelatinized and fixed with 4% paraformaldehyde/PBS. Whole embryo and section images were taken by using the software QCapture.

Cell Culture and Transfection Conditions—Human cardiac fibroblasts from a normal 18-year-old individual were obtained from a commercial source (Innoprot) and cultured as previously described (21, 22). In brief, cells were grown in Iscove's modified Dulbecco's medium (Lonza), supplemented with 20% FBS (Hyclone), 10 ng/ml basic fibroblast growth factor (R&D), 1% penicillin/streptomycin (Thermo Fisher Scientific), and 1% L-glutamine (Lonza). Cells were passaged 1:3 twice a week, and experiments were performed between passages 4 and 6.

CASZ1b overexpression in human cardiac fibroblasts was achieved by transfection of 5 μg of CASZ1b-GFP plasmid (Origene) or an equivalent amount of control vector using an Amaxa P1 primary cell 4D Nucleofector kit (Lonza). All the analyses were performed using four independent CASZ1b nucleofection experiments in different human cardiac fibroblast cell preparations.

HL-1 cells, a cardiac muscle cell line derived from mouse atrial cardiomyocyte tumor lineage, were maintained as described previously (23). Briefly, cells were cultured on gelatin (0.02%, w/v)/fibronectin (10 μg/ml)-coated flasks or plates. The cells were maintained in Claycomb medium (Sigma-Aldrich) supplemented with 10% fetal bovine serum (Invitrogen), 2 mM L-glutamine, 0.1 mM norepinephrine, 100 unit/ml penicillin, and 100 μg/ml streptomycin (Thermo Fisher Scientific).

HL-1 cells were plated in 12-well plates. For knockdown experiments, 65 nM all stars negative control siRNA (Qiagen catalog number SI03650318) or murine *Casz1* siRNA (Qiagen catalog number SI00970529) was transfected using Lipofectamine 2000 (Invitrogen) according manufacture's instruction. For overexpression experiment, 2 μg pCMVTag2A-CASZ1b plasmids (11) or empty vector pCMVTag2A were transfected using Lipofectamine 2000 (Invitrogen). Two days later cells were collected for subsequent experiments. This experiment has been repeated twice.

Primary cardiomyocytes were isolated from E14.5 embryo hearts as reported (24) without preplating to remove the fibroblast cells. Cardiomyocytes were cultured on laminin coated 4-well chambers or 24-well plates with coverslip for 2 days before immunofluoresence staining.

Section Immunofluorescence and H&E Staining—These techniques were performed as previously described (25, 26). Embryos were fixed with 4% paraformaldehyde/PBS at 4C overnight. After fixation, the embryos were either placed in 70% ethanol and then embedded in paraffin compound or sunk in 30% sucrose/PBS at 4 °C and then embedded in OCT compound. 5-μm-thick paraffin sections of embryo hearts were used for H&E staining or immunofluoresence staining. Paraffin embedding and H&E staining were performed by Histoserv Inc. For immunostaining studies, histologic sections were deparaffinized in xylene and rehydrated to PBS. Staining was performed using anti-MF 20 antibody (developmental studies hybridoma bank mouse antibody, 1:30 overnight at 4 °C), pHH3 antibody (Sigma-Aldrich H9908, rat antibody, 1:300 overnight at 4 °C), desmin antibody (Millipore MAB3430, mouse antibody, 1:200 overnight at 4 °C), and α-actinin (Abcam ab9465, mouse antibody, 1:100 overnight at 4 °C) to detect their expression. For immunofluorescent detection, either Alexa 488- or Alexa 568-conjugated secondary antibodies (Thermo Fisher Scientific 1:250, 1 h at room temperature) were used. Stained sections were imaged using a Zeiss ApoTome 2 microscopy, a

TABLE 2
Real time PCR primers

Primer name[a]	Forward primer sequence	Reverse primer sequence
mGAPDH	AACTTTGGCATTGTGGAAGG	ATGCAGGGATGATGTTCTGG
mCasz1–2935	CTGCCTCCATCATTGAGAGAAT	TCATTACTGGGATCCTTCACG
mACAN	CCTGTGGTGGGGACAAACCT	CCCCACCTGAGTGACGATCC
mCKM	TTGACAAGCCCGTGTCACCT	CAGAAGCGGCGGAAAACCTC
mACTA1	GCCAGAGTCAGAGCAGCAGA	TTGCTCTGGGCCTCATCACC
mTNNI2	TCGGAGGGTGCGTATGTCTG	GCAGGTCCCGTTCCTTCTCA
mTNNT1	CCAAACCCAGCCGTCCTGT	TCGCCTCTCAATGCGGTCTT
mITGA7	CTCCGTTCGGGCTCATGTCT	CCCTCTCAGATCGCATGGCA
mITGA10	CCGCTAGGCTGCTGGTAGTT	CTGTCAGCGCAGCTTCATCG
mCOL2A1	CAGCTGTCTGCAGAATGGGC	GACAGCACTCTCCGAAGGGG
mABCC9	CCCGCTGAGACGGAAGACAT	TTCCACAACCCACTTGGCCT
mCACNA1D	TTCCGCTCGGTGGCTGTATT	TCCTCCGTGCTTTCTACCGC
mKCND2	CTGGGGTATGGCGACATGGT	GTAGGCATTTGCACTCCCGC
mATP1A3	TCATCAGTCTGAACGCCGCT	GACCCTGCACGCAGTCAGTA
mTP63	AGCAAGTATCGGACAGCGCA	TCGATCGTGTGCTGAGGGAG
mEdn1	AGGTCCAAGCGCTGTTCCTG	TGCCTGGTCTGTGGCCTTAT
mNEFL	GAAGCCTGCCGGGGTATGAA	GAGCCTGGTCTCTTCGCCTT
mTGFB3	CGACCGGATGAGCACATAGC	AGGTGTGACATGGACAGTGGA
mDCC	GGCTATGGTGTTGGCAGTCC	ATCAACGGGGTCAGTGGGAT
mSIK1	GTCACCAAAACGCAGGTTGC	CAAGTGCCCGTTGGAAGTCA
hGADPH	GGGACGCTTTCTTTCCTTTC	GCTGCCCATTCATTTCCTT
hCASZ1	CAAAACAGACTCCATCACCACG	GTGCTGGCTGCCCGAGAAC
hACTA1	TCCTCCCTGGAGAAGAGCTA	GGTCCTTGCGGATATCAATG
hTNNT1	GCAGAACAGAAGCGTGGTAA	GCCATCAGGTCGAACTTCTC
hCKMT1A	GTCTCTAGCCGCTGGGTTTC	AGCCGTGCATAGACTGCTG
hITGA10	GTTCTTGCCCCTGGTGTTCCT	CCTAAGTGGCCCTTGGCACAT
hACAN	ACCTGAGCAGCATCGTCACC	AGTCCTCTCCAGCGGCAAAA
hTGFB3	CGTGCCGTGAACTGGCTTC	AGCACCTCGGCTTGTCTTCT

[a] Primer names starting with "m" represent mouse genes, and primer names starting with "h" represent human genes.

Leica TGS SP5 confocal microscope or a Nikon Eclipse TE300 microscope.

TUNEL Assays—Apoptosis (TUNEL) assays were performed on paraffin sections using DeadEnd Fluorometric TUNEL system kit (Promega) and counterstained with DAPI. Stained sections were imaged using a Zeiss ApoTome 2 microscopy.

Whole Mount Staining of the Embryo Heart—Whole mount staining was performed as described previously (26, 27). In brief, hearts were dissected from E14.5 embryos, fixed in 4% paraformaldehyde/PBS at 4 °C overnight, and then placed in 70% ethanol at 4 °C for extended storage. Staining was performed using anti-β-galactosidase antibody (Cappel, rabbit antibody 1:500 overnight at 4 °C) to detect Casz1, and using phalloidin-Alexa 488 (Invitrogen, 1:40, 20 min at room temperature) to detect heart structure. For immunofluorescent detection, either Alexa 488- or Alexa 568-conjugated secondary antibodies (Thermo Fisher Scientific 1:250, 1 h at room temperature) were used. All confocal microscopy was carried out on a Leica TCS SP5 confocal microscope.

Western Blot—Western blot was performed as previously described (13, 28). In brief, to extract protein from heart, whole hearts were dissected from E14.5 embryos and dissolved in radioimmune precipitation assay buffer. Protein was extracted using Bioruptor sonicator with protein extraction beads at high power for 10 cycles (30 s on and 30 s off). Proteins were electrophoresed in a 4–20% polyacrylamide gel (Bio-Rad) and transferred electrophoretically to nitrocellulose membranes (Schleicher & Schuell). Rabbit anti-GAPDH (Santa Cruz, 1:4000) and rabbit anti-Casz1 (Rockland, 1:1000) were used to detect GAPDH and Casz1 protein level in heart. To extract protein from human cardiac fibroblasts, cells were lysed in Laemmli buffer 5 days after CASZ1b transfection. Forty micrograms of protein lysate was loaded onto gels to assess CASZ1 protein levels. Membrane has been probed with CASZ1 antibody (polyclonal, 1:500 Santa Cruz) and α-tubulin antibody (monoclonal, 1:4000 Cell Signaling).

RNA Isolation and cDNA Analysis by qRT-PCR—Total RNA was extracted from *Casz1*$^{+/+}$ and *Casz1*$^{\beta geo/\beta geo}$ hearts at E12.5, or human cardiac fibroblast cells, or mouse HL-1 cardiomyocytes using the RNeasy mini kit (Qiagen) as per the manufacturer's protocol. Quantitative measurements of different gene levels were obtained using Step One Plus real time PCR (Applied Biosystems) as described previously (11, 28). The expression of mouse *GAPDH* mRNA was used as internal control for heart or HL-1 cells, and mRNA expression of human *GAPDH* was used as internal control for human cardiac fibroblast cells. The primer sequences were listed in Table 2. The experiment was repeated at least once in triplicate.

The Oligonucleotide Microarray—Affymetrix Mouse MO gene 2.0 ST arrays were used to determine genes regulated by *Casz1* in embryonic murine hearts. Total RNA was extracted from three *Casz1*$^{+/+}$ and three *Casz1*$^{\beta geo/\beta geo}$ hearts at E12.5. Among these hearts, one *Casz1*$^{+/+}$ heart and one *Casz1*$^{\beta geo/\beta geo}$ heart were from the same litter as a pair, and hearts from three different litters were used as biological replicates. Array hybridization, chemiluminescence detection, and image acquisition were performed by Laboratory of Molecular Technology of NCI-Frederick core facility. Raw CEL files were uploaded onto Partek Genomics Suite v6.6 for data analysis. A Fisher's test was applied to identify differently expressed features by comparing *Casz1*$^{\beta geo/\beta geo}$ and *Casz1*$^{+/+}$ samples. The filter thresholds for a p value of <0.05 and an absolute fold change of 1.5 were imposed to retrieve a list of significantly differentially expressed genes. The differentially expressed genes were uploaded onto ingenuity pathway analysis (IPA) for further data analysis.

Statistical Analyses—Statistical analyses of the data were performed using a t test or CHITEST with $p < 0.05$ considered

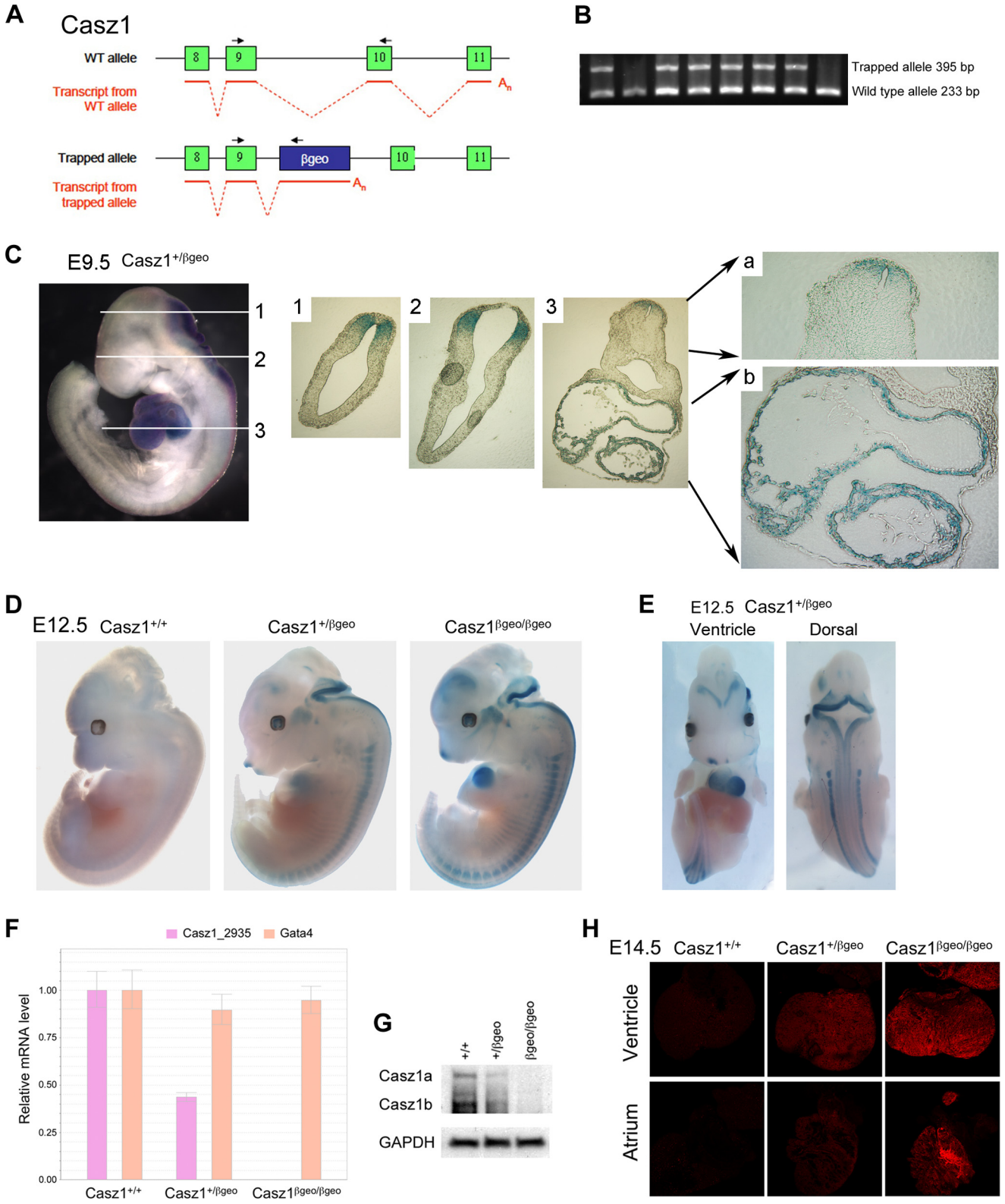

FIGURE 1. ***Casz1* expression pattern during mouse embryogenesis.** *A*, cartoon of the *Casz1* gene trap that inserted with a βgeo reporter after *Casz1* exon 9 resulting in a truncated *Casz1*. *B*, genotyping of *Casz1*-trapped mice by RT-PCR. *C*, whole mount X-gal staining (*blue*) of E9.5 $Casz1^{+/\beta geo}$ embryos shows that Casz1 was expressed in the hindbrain, neural tube, and heart, which are further demonstrated by dissected embryo sagittal sections 1, 2, and 3 (100× magnification). Sagittal section 3b (200× magnification) shows that Casz1 was expressed in the cardiomyocytes. *D* and *E*, whole mount X-gal staining of E12.5 $Casz1^{+/+}$, $Casz1^{+/\beta geo}$, and $Casz1^{\beta geo/\beta geo}$ embryos showed that *Casz1* is expressed in the eye, dorsomedial telencephalon, cranial ganglia, nasal placode, somite, neural tube, and heart. *F*, real time PCR to detect wild type *Casz1* allele and Gata4 mRNA levels in E12.5 hearts. *G*, the protein levels of Casz1a/Casz1b and GAPDH were visualized by immunoblotting E14.5 whole heart lysate with anti-Casz1 antibody and anti-GAPDH antibody. *H*, whole mount anti-β-galactosidase staining (*red*) of E14.5 $Casz1^{+/+}$, $Casz1^{+/\beta geo}$, and $Casz1^{\beta geo/\beta geo}$ hearts.

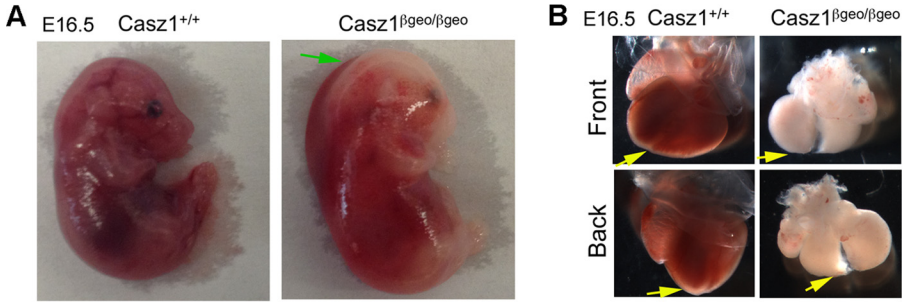

FIGURE 2. **Phenotype of *Casz1*$^{\beta geo/\beta geo}$ embryo and heart at E16.5.** *A*, E16.5 *Casz1*$^{\beta geo/\beta geo}$ embryo shows evidence of edema and broad areas devoid of blood (*green arrow*). *B*, the E16.5 *Casz1*$^{\beta geo/\beta geo}$ hearts were morphologically different compared with wild type heart (compare the regions targeted by the *yellow arrows*). (Note the lack of blood in the *Casz1*$^{\beta geo/\beta geo}$ heart occurred after surgery.)

significant. The values in the graphs are expressed as means ± S.D. or S.E. The statistical tests were two-sided.

RESULTS

Expression Pattern of Casz1 during Embryonic Development—Casz1 gene encodes two major isoforms: full-length Casz1a and a shorter isoform Casz1b, with both isoforms sharing the same 5′-proximal "promoter" region and the first 16 exons. In the *Casz1* knock-out mouse, the *Casz1* gene trap inserts a βgeo reporter after *Casz1* exon 9 (Fig. 1*A*), resulting in a truncated *Casz1* allele in which 10 of the 11 zinc fingers of full-length *Casz1* are lost. The zinc fingers are critical domains for Casz1 function (14). Using primers specific for the WT (*Casz1*$^{+/+}$) allele and the trapped allele, we found that *Casz1*$^{+/+}$ mice only have the unaltered *Casz1* allele, whereas *Casz1* heterozygous (*Casz1*$^{+/\beta geo}$) mice have both the WT allele and the trapped allele (Fig. 1*B*). Among 183 progeny of male *Casz1*$^{+/\beta geo}$ and female *Casz1*$^{+/\beta geo}$ mice, 63 (35.4%) mice are WT (*Casz1*$^{+/+}$) and 120 (64.6%) mice are heterozygous (*Casz1*$^{+/\beta geo}$), but none are homozygous (*Casz1*$^{\beta geo/\beta geo}$). This indicates that *Casz1* mutation in both alleles results in embryonic lethality. Timed mating results showed that the embryonic lethality occurred at E17.5; no live *Casz1*$^{\beta geo/\beta geo}$ embryos were observed after E17.5.

To determine the role of *Casz1* during embryogenesis, we first investigated the expression pattern of *Casz1* during embryonic development. In *Casz1* trapped embryos, the βgeo reporter was under the control of endogenous *Casz1*, and therefore X-gal staining or anti-β-galactosidase staining could be used to characterize the pattern of *Casz1* expression during embryonic development. Whole mount X-gal staining of E9.5 embryos showed that Casz1 was expressed in the neural tube and heart (Fig. 1*C*, *left panel*), which was consistent with previously reported *in situ* hybridization analysis results (10). Transverse sectioning showed that Casz1 was expressed in the hindbrain and dorsal aspect of the spinal cord, as well as in cardiomyocytes of the heart (Fig. 1*C*, *right panel*). Whole mount X-gal staining of E12.5 embryos showed that Casz1 was expressed in the eye, dorsomedial telencephalon, cranial ganglia, nasal placode, somite, neural tube, and heart (Fig. 1, *D* and *E*). To confirm the expression of Casz1 in the heart, total RNA was extracted from the entire heart of E12.5 embryos, and real time PCR was performed using primers that only recognize the wild type allele but not the trapped allele. Consistent with X-gal staining, real time PCR results showed that *Casz1* mRNA was expressed in the heart (Fig. 1*F*). Endogenous *Casz1* mRNA was detected in the heart of *Casz1*$^{+/+}$ embryos, a half amount of *Casz1* mRNA level was detected in the heart of the *Casz1*$^{+/\beta geo}$ embryo, and the *Casz1* mRNA level was undetectable in the heart of the *Casz1*$^{\beta geo/\beta geo}$ embryo. Gata4, an early cardiac marker, was expressed at similar levels in these hearts (Fig. 1*F*). Western blot analysis of E14.5 hearts using an anti-Casz1 antibody demonstrated the protein expression of both Casz1a and Casz1b isoforms in WT hearts but not in *Casz1*$^{\beta geo/\beta geo}$ heart, confirming the deficiency of Casz1 in the knock-out mouse (Fig. 1*G*). Whole mount staining of the E14.5 hearts using anti-β-galactosidase antibody showed that Casz1 was expressed in the ventricles and atriums of the heart (Fig. 1*H*).

Loss of Casz1 in the Embryos Leads to an Abnormal Myocardium Development—The *Casz1*$^{\beta geo/\beta geo}$ embryos at E16.5 showed a swollen phenotype with accumulation of fluid in subcutaneous regions, which is often associated with heart failure in embryos (Fig. 2*A*). The E16.5 *Casz1*$^{\beta geo/\beta geo}$ heart is morphologically different in shape, with the ventricle apex being spherical and not the normal triangular in shape (Fig. 2*B*).

Edema was detected in *Casz1*$^{\beta geo/\beta geo}$ embryos at E15.5 but not seen in WT or *Casz1*$^{+/\beta geo}$ embryos (Fig. 3*A*). E15.5 embryos were transverse dissected, and H&E staining was performed to investigate heart development. Unlike the WT heart or *Casz1*$^{+/\beta geo}$ heart, the compact myocardium (free wall) of both ventricles and the septum in the *Casz1*$^{\beta geo/\beta geo}$ heart was hypoplastic (Fig. 3, *B–D*, *column 1*). At higher magnification (Fig. 3, *B–D*, *columns 2* and *4*), it was clear that E15.5 *Casz1*$^{\beta geo/\beta geo}$ heart has abnormal myocardium with significant thinning and less compact of walls in both the left and right ventricles, and the septum was also thinner and less compact (Fig. 3, *B–D*, *column 3*). Moreover, more blood cells accumulated in the liver of the *Casz1*$^{\beta geo/\beta geo}$ embryo when compared with the livers of the *Casz1*$^{+/+}$ and *Casz1*$^{+/\beta geo}$ embryos (Fig. 3*E*), a finding also consistent with functional defects in the *Casz1*$^{\beta geo/\beta geo}$ heart.

We further focused on E14.5 embryos heart, at a time when the ventricle septation is complete. Edema was also detected in some of the E14.5 *Casz1*$^{\beta geo/\beta geo}$ embryos, but not as clear as in E15.5 embryos. Indeed, the skin on the backs of the *Casz1*$^{\beta geo/\beta geo}$ embryos exhibits an enlarged lymphatic network, although sprouting lymphangiogenesis appeared to occur normally at the lymphatic vascular front (Fig. 4). This lymphatic phenotype may

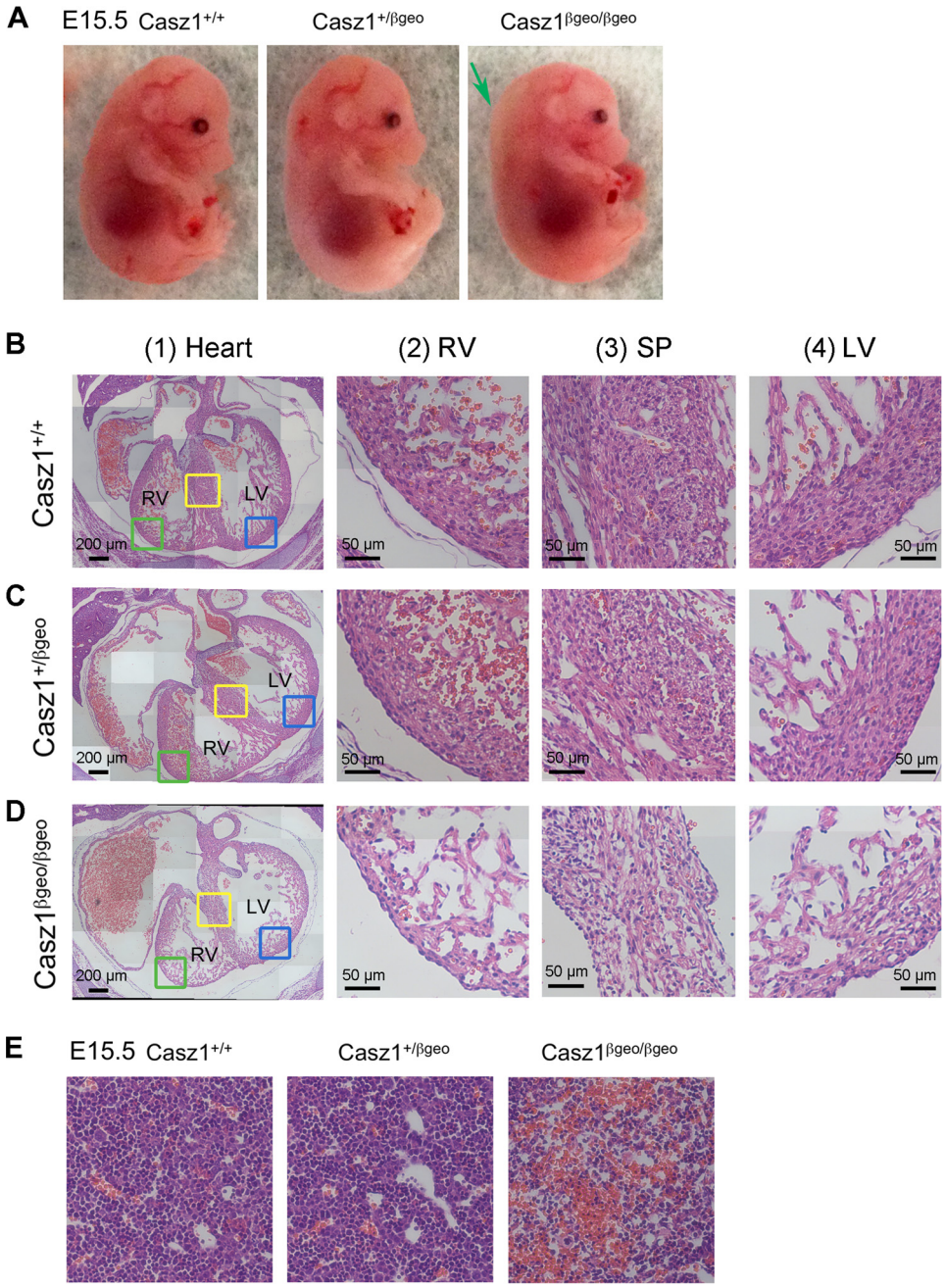

FIGURE 3. **Hypoplasia in the myocardium of *Casz1*$^{\beta geo/\beta geo}$ heart.** *A*, phenotype of *Casz1*$^{+/+}$, *Casz1*$^{+/\beta geo}$ and *Casz1*$^{\beta geo/\beta geo}$ E 15.5 embryos. The edema was seen at the neck region on the back of *Casz1*$^{\beta geo/\beta geo}$ embryos but not other embryos (green arrow). *B–D*, *column 1*, H&E staining of transverse sections of E15.5 *Casz1*$^{+/+}$ (*B1*), *Casz1*$^{+/\beta geo}$ (*C1*), and *Casz1*$^{\beta geo/\beta geo}$ (*D1*) embryos. *Column 2*, right ventricle (*RV*) magnification of the respective *green squares* from *column 1*. *Column 3*, septum (*SP*) magnification of respective *yellow squares* from *column 1*. *Column 4*, left ventricle (*LV*) magnification of respective *blue squares* from *column 1*. *E*, representative photomicrographs indicate accumulation of blood cells in the liver of the *Casz1*$^{\beta geo/\beta geo}$ embryo (*right panel*) but not in the *Casz1*$^{+/+}$ (*left panel*) or *Casz1*$^{+/\beta geo}$ (*middle panel*) embryo.

be a secondary defect of loss of Casz1 because β-galactosidase staining did not show the expression of Casz1 in lymphatic endothelial cells.

The *Casz1*$^{\beta geo/\beta geo}$ heart was morphologically distinct from the *Casz1*$^{+/\beta geo}$ or *Casz1*$^{+/+}$ heart, with the left ventricle apex being spherical and not the normal triangular in shape (Fig. 5*A*). Consecutive sectioning of the E14.5 embryos showed that three of three *Casz1*$^{\beta geo/\beta geo}$ hearts had four chambers, four valves, and normal outflow tract alignment, but the ventricular septum was abnormal, with ventricle septal defects (Fig. 5*B*). The compact myocardium of both ventricles and the septum of the E14.5 *Casz1*$^{\beta geo/\beta geo}$ heart were hypolastic, although they were not as obvious as the E15.5 *Casz1*$^{\beta geo/\beta geo}$ hearts (Fig. 5*B*, *top panels*). Higher magnifications clearly showed the ventricular septal defect in *Casz1*$^{\beta geo/\beta geo}$ heart but not in *Casz1*$^{+/+}$ heart (Fig. 5*B*, *bottom panels*).

Casz1 Deficiency in Heart Leads to the Decrease of Cardiomyocyte Proliferation—To investigate whether the hypoplasia of *Casz1*$^{\beta geo/\beta geo}$ compact myocardium was caused by reduced cardiomyocyte proliferation, we stained the transverse

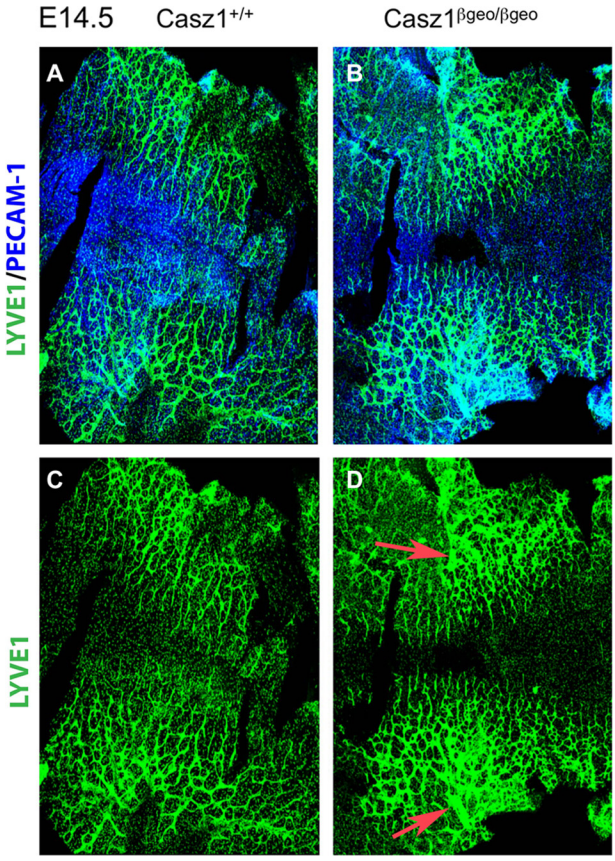

FIGURE 4. **E14.5 *Casz1*$^{\beta geo/\beta geo}$ embryos exhibit abnormal lymphatic networks.** Whole mount triple immunofluorescence labeling of back skin with antibodies to the lymphatic endothelial cells marker, LYVE-1 (*green*) and pan-endothelial cells marker, PECAM-1 (*blue*) in the *Casz1*$^{\beta geo/\beta geo}$ embryos (*B* and *D*) and control littermates (*A* and *C*). Compared with the control littermates, *Casz1*$^{\beta geo/\beta geo}$ embryos showed the enlarged and disorganized lymphatic vessel morphogenesis (*red arrows*).

sections of E14.5 *Casz1*$^{+/+}$ and *Casz1*$^{\beta geo/\beta geo}$ heart for the cardiomyocyte marker MF-20 (the heavy chain of striated myosin II) and for phosphorylated histone H3 (pH3), a marker of the M phase of the cell cycle (Fig. 5*C*, *left panels*). Loss of *Casz1* led to a more than 3-fold decrease in the fraction of pH3 positive cardiomyocytes compared with *Casz1*$^{+/+}$ hearts (Fig. 5*C*, *right panel*), which is consistent with a decrease in cell proliferation contributing to the hypoplasia in the *Casz1*$^{\beta geo/\beta geo}$ hearts. To determine whether apoptosis also contributes to the hypoplasia of the compact myocardium in *Casz1*$^{\beta geo/\beta geo}$ heart, we performed a tunnel assay and found that there was no increase in the number of apoptotic cells in *Casz1*$^{\beta geo/\beta geo}$ heart compared with *Casz1*$^{+/+}$ hearts at the time evaluated (Fig. 5*D*).

Casz1$^{\beta geo/\beta geo}$ *Heart Exhibits Disorganized Myofiber Orientation and Cell Alignment*—Because the *Casz1*$^{\beta geo/\beta geo}$ heart was morphologically distinct from the *Casz1*$^{+/\beta geo}$ or *Casz1*$^{+/+}$ heart (Fig. 5*A*), we next investigated whether loss of *Casz1* affects myofiber organization and cellular alignment. E14.5 whole mount hearts were stained with phalloidin-Alexa 488 to visualize F-actin and the arrangement of the thin filaments. The immunofluoresence analysis revealed that the myocytes within the heart wall of E14.5 *Casz1*$^{+/+}$ heart were well aligned; however, disruption of the fiber orientation and cell alignment were observed in both the left ventricle and the right ventricle of *Casz1*$^{\beta geo/\beta geo}$ heart; representative images of the left ventricles are shown in Fig. 6.

Casz1$^{\beta geo/\beta geo}$ *Heart Has an Abnormal Gene Expression Pattern*—To understand the underlying mechanisms contributing to the *Casz1*$^{\beta geo/\beta geo}$ heart defect, we analyzed the transcriptome of the E12.5 *Casz1*$^{+/+}$ and *Casz1*$^{\beta geo/\beta geo}$ hearts. Genome-wide RNA expression-profiling analysis of *Casz1*$^{\beta geo/\beta geo}$ heart versus *Casz1*$^{+/+}$ heart showed that the expression level of 187 Affymetrix probe set IDs were significantly changed (decreased or increased greater than 1.5-fold, $p < 0.05$). Among these probe set IDs, 148 mapped to known gene ID with 53 genes being down-regulated and 95 genes up-regulated in *Casz1*-deficient heart (Fig. 7*A* and supplemental Table S1). Gene ontology and IPA assays showed that three groups of altered genes might contribute to the *Casz1*$^{\beta geo/\beta geo}$ heart abnormalities. These include 1) cell adhesion molecules, 2) genes involved in muscular system development and function, and 3) ion channel genes.

Partek gene ontology analysis of these 148 genes showed that "biological adhesion" genes are one of the most significantly enriched group of genes with enrichment score of 4.5 and enrichment *p* value of 0.01 (Fig. 7*B*). These genes include *ACAN*, aggrecan; *ITGA7*, integrin α7; *ITGA10*, integrin α10; *ITGB8*, integrin β8; *CDH6*, cadherin 6; *COL2A1*, collagen, type II α1; and *COL8A1*, collagen type VIII α1. We validated the microarray findings by using quantitative real time PCR (qRT-PCR) to assay some of these cell adhesion genes with known cardiac expression. The qRT-PCR results showed that *ACAN*, *ITGA7*, *ITGA10*, and *COL2A1* mRNA levels were significantly increased in *Casz1*$^{\beta geo/\beta geo}$ heart (Fig. 7*D*). These genes are known to be important for cell organization and tissue morphogenesis.

IPA analysis of *Casz1* target genes showed that in the physiological system development and function categories, genes involved in skeletal and muscular system development and function are the most significantly enriched genes (Fig. 7*C*, *left panel*). These genes include *TGFB3*, transforming growth factor, β3; *CKM*, creatine kinase, muscle; *ACTA1*, skeletal actin α 1; *CASQ1*, calsequestrin 1, fast-switch skeletal muscle; *TNNI2*, troponin I type 2, skeletal, fast; and *TNNT1*, troponin T type 1, skeletal, slow. These are muscle development and/or muscle contraction genes or genes encoding cell structure proteins. Consistent with the microarray results, the qRT-PCR results showed that representative gene *CKM*, *ACTA1*, *TNNI2*, and *TNNT1* mRNA levels were significantly decreased in *Casz1*$^{\beta geo/\beta geo}$ heart (Fig. 7*D*).

In addition to the alterations in expression of the cell adhesion and muscle development genes in *Casz1*$^{\beta geo/\beta geo}$ heart, we found dysregulation of multiple ion channel genes in *Casz1*$^{\beta geo/\beta geo}$ heart (Fig. 7*C*, *right panel*). Some of these genes, especially the potassium and calcium channel genes, have the potential to affect the conduction system function in the heart, whereas some of them have been reported to affect cardiac arrhythmia. These genes include *ABCC9*, ATP-binding cassette, subfamily C, member 9 (part of an ATP-dependent potassium channel); *ATP1A3*, ATPase, Na^+/K^+ transporting, α3 polypeptide; *CACNA1D*, calcium channel, voltage-dependent, L type, α1D subunit; *KCNK3*, potassium channel, subfamily K,

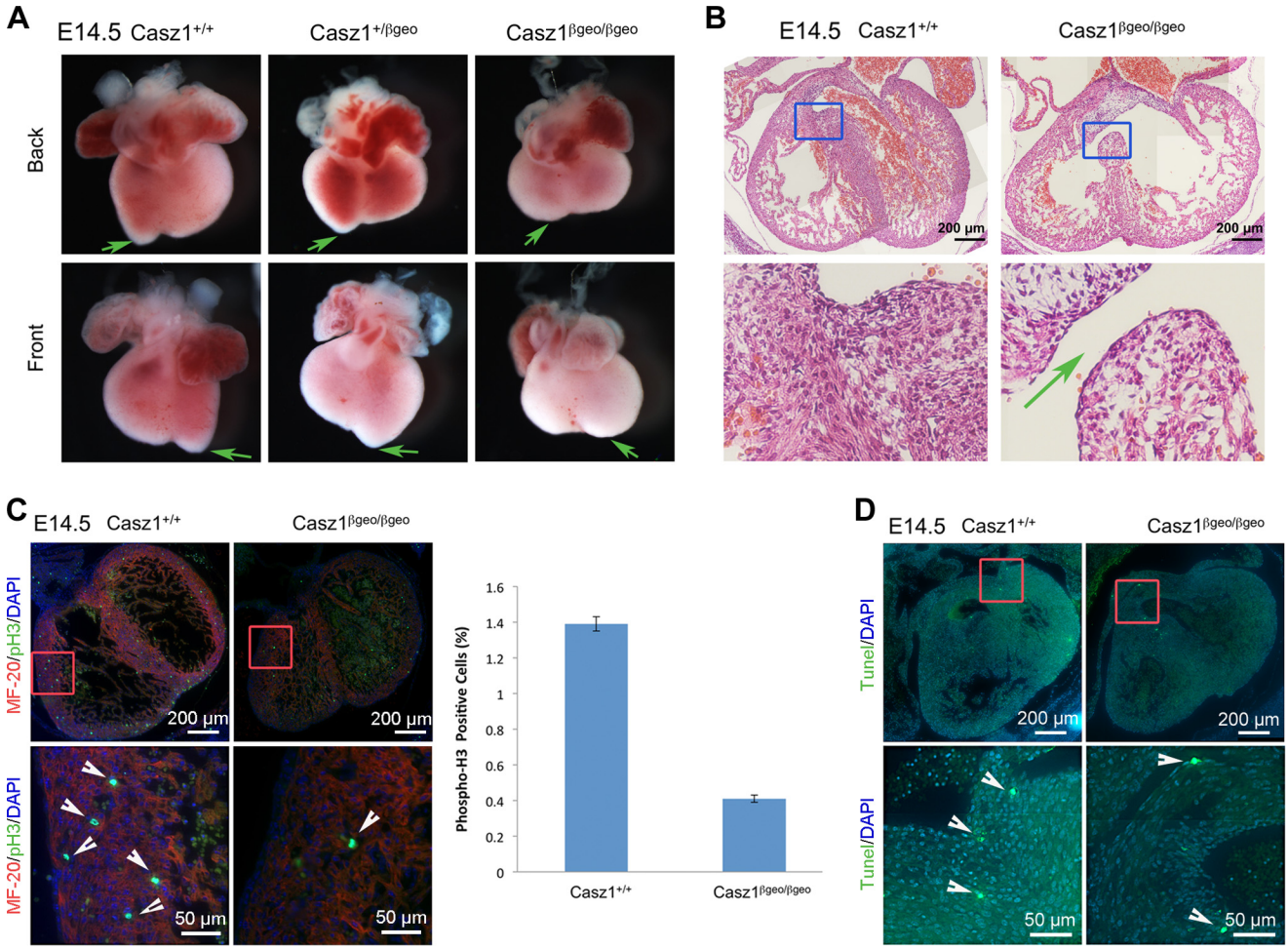

FIGURE 5. **Decreased proliferation in *Casz1*$^{\beta geo/\beta geo}$ heart.** *A*, the E14.5 *Casz1*$^{\beta geo/\beta geo}$ hearts were morphologically different compared with the *Casz1*$^{+/\beta geo}$ or wild type heart (compare the *green arrow* targeted region). *B*, lower magnification of H&E staining of transverse sections from E14.5 embryos (*upper panels*). The *lower panels* represent a magnification of the regions that are depicted in the *blue squares* in the *upper panel*. The *green arrow* denotes the septal defect apparent in the serial sectioning of the *Casz1*$^{\beta geo/\beta geo}$ heart compared with the *Casz1*$^{+/+}$ heart. *C*, paraffin sections from E14.5 hearts from *Casz1*$^{+/+}$ and *Casz1*$^{\beta geo/\beta geo}$ hearts were immunostained with antibodies for MF20 (*red*) and the mitosis marker phosphohistone H3 (*pH3*, *green*). The nuclei were stained with DAPI (*blue*; *left top panels*, original overview; *left bottom panels*, high magnification). In the high magnification images, *arrows* indicate pH3^{+} cells. The graph (*right panel*) represents the relative percentage of pH3 positive cells compared with the total number of DAPI positive *Casz1*$^{\beta geo/\beta geo}$ or *Casz1*$^{+/+}$ cardiomyocytes from at least five sections from each embryo. The *Casz1*$^{\beta geo/\beta geo}$ cardiomyocytes proliferate significantly slower than *Casz1*$^{+/+}$ cardiomyocytes ($p < 0.00001$). *D*, tunnel staining (*green*) was performed using E14.5 heart paraffin sections (*upper panels*), and nuclei were stained with DAPI (*blue*). The *lower panels* represent magnified areas delineated in the *red squares* in the *upper panels*. There was no significant difference in the number of apoptotic cells observed in *Casz1*$^{\beta geo/\beta geo}$ cardiomyocytes compared with *Casz1*$^{+/+}$ cardiomyocytes.

member 3; and KCND2, potassium voltage-gated channel, shal-related subfamily, member 2. Consistent with the microarray results, qRT-PCR results showed that representative gene *CACNA1D* and *ATP1A3* mRNA levels were significantly increased, whereas *ABCC9* and *KCND2* mRNA levels were significantly decreased in *Casz1*$^{\beta geo/\beta geo}$ heart (Fig. 7*D*).

Because loss of *Casz1* led to a decrease of cardiomyocyte proliferation, we assessed whether *Casz1* affects the expression of genes controlling cell cycle and cell proliferation. IPA analysis of *Casz1* target gene showed that genes involved in cell cycle and cellular growth were significantly enriched (Fig. 8*A*). These genes include *EDN1*, endothelin-1; *NEFL*, neurofilament, light polypeptide; *TGFB3*, transforming growth factor β3; *DCC*, deleted in colorectal carcinoma; and *SIK1*, salt-inducible kinase 1. Consistent with the microarray results, the changes in the expression of these genes were confirmed by qRT-PCR (Fig. 8*B*). In the microarray data, we found that TP63, tumor protein 63, a classic cell cycle and growth regulation gene, was up-regulated by 1.4-fold in *Casz1* knock-out heart, which was not included in the initial analysis because the cut-off was set as > or <1.5-fold. However, qRT-PCR results confirmed the up-regulation of TP63 in *Casz1*-deficient heart (Fig. 8*B*). Thus the dysregulation of genes involved in cell cycle and cell growth regulation in *Casz1*-deficient heart may contribute to a decrease in cardiomyocyte proliferation.

Validation of Casz1 Target Genes in Cellular Models—To provide additional evidence for *Casz1*-dependent gene expression in heart, we performed gain and loss of function studies in cellular models. For overexpression expression experiments we used the human CASZ1b cDNA construct because it is the most evolutionarily conserved isoform (11, 14). First, we used human cardiac fibroblasts whose level of Casz1 expression is not detectable by routine qRT-PCR. After overexpression of Casz1 in cardiac fibroblast cells, the muscular system developmental gene *TNNT1*, *CKM*, and the contract fiber gene *ACTA1* mRNA were significantly up-regulated, whereas the cell adhe-

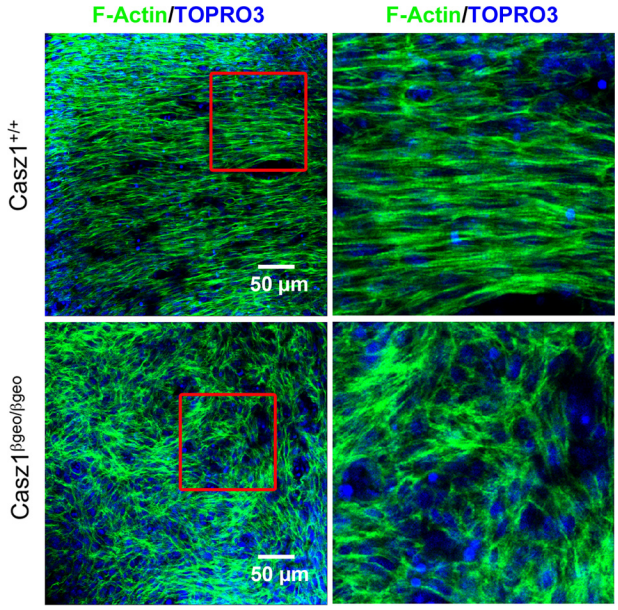

FIGURE 6. **Disorganized fiber orientation in *Casz1*$^{\beta geo/\beta geo}$ heart.** To visualize thin filaments, *Casz1*$^{+/+}$ and *Casz1*$^{\beta geo/\beta geo}$ E14.5 hearts were stained with phalloidin-488 (*green*) to detect F-Actin and co-stained with TOPRO3 to show cell nuclei. The *left panels* show the co-staining results of the left ventricles of the hearts. The *right panels* represent magnified areas delineated in the *red squares* in the *left panels*. Enlarged images showed complete disruption of the fiber orientation/cell alignment in the left ventricle (*LV*) of *Casz1*$^{\beta geo/\beta geo}$ heart.

sion gene *ACAN*, *ITGA10*, and cell growth regulation gene *TGFB3* were significantly decreased (Fig. 9*A*, *panel c*). In another model, the cardiac muscle cell line HL-1 retains phenotypic characteristics of cardiomyocytes and expressed Casz1. Real time PCR analysis showed that after knockdown of *Casz1* expression, contractile fiber gene *ACTA1* mRNA levels were significantly decreased, whereas the cell adhesion gene *ITGA10* and cell growth regulation gene *TGFB3* mRNA levels were significantly increased (Fig. 9*B*, *panel a*). Overexpression of CASZ1b significantly increased *ACTA1* mRNA level and decreased *IGTA10* gene mRNA levels, although overexpression of CASZ1b did not lead to the significant decrease in *TGFB3* mRNA levels (Fig. 9*B*, *panel c*). These results validated our microarray data and demonstrated that in two cellular models *in vitro*, *Casz1* regulated some of the genes that were regulated in hearts *in vivo*.

Loss of Casz1 Affects Sarcomeric Organization—To gain insights from the microarray data, we further performed gene set enrich analysis (GSEA) using the whole microarray gene list. GSEA is able to determine whether an *a priori* defined set of genes shows a statistically significant difference between *Casz1*$^{+/+}$ and *Casz1*$^{\beta geo/\beta geo}$ heart. The results showed that the "contractile fiber" genes (genes which encode muscle structural and regulatory proteins) were negatively enriched in *Casz1*$^{\beta geo/\beta geo}$ heart, and the expression level of these genes decreased in *Casz1*$^{\beta geo/\beta geo}$ heart (Fig. 10*A*, *panels a* and *b*). Similarly, the contractile fiber genes were also significantly enriched (Fig. 10*A*, *panel c*). Contractile myofibers are composed of contractile units (sarcomeres) consisting of A band, I band, M band, and Z disc (Z line). To investigate whether the loss of *Casz1* affected the organization of contractile fibers, we stained the transverse section of the E14.5 hearts with anti-desmin antibody. Desmin forms a network of filaments that extends across the myofibril and surrounds Z discs. Immunofluoresence analysis revealed a clear striated pattern for desmin labeling in cardiomyocytes of the trabecular region of *Casz1*$^{+/+}$ heart. A striated pattern of desmin labeling in the *Casz1*-deficient heart could be detected, but it was not as pronounced, and the Z line density was lower (Fig. 10*B*). Electron microscopy of heart sections from *Casz1*$^{\beta geo/\beta geo}$ embryos confirmed that a normal sarcomeric structure could exist but did not enable an enumeration of whether there were different degrees of formation.

To further evaluate and quantify how the loss of *Casz1* affected myofiber organization, we cultured E14.5 cardiomyocytes *in vitro* and stained the cells with anti-α-actinin antibody (Fig. 11). α-Actinin is present at the Z line of the sarcomere. The cells were co-stained with phalloidin-Alexa 488 to detect F-actin. Immunofluorescence analysis revealed a clear striated pattern for α-actinin labeling in over 80% of cardiomyocytes from Casz1$^{+/+}$ heart, but less than 50% of cardiomyocytes from *Casz1*$^{\beta geo/\beta geo}$ heart exhibited a clear striated pattern of α-actinin labeling (Fig. 11, *A*, *left panels*, and *B*). Consistently immunofluorescence analysis revealed a clear striated pattern for F-actin labeling in cardiomyocytes from *Casz1*$^{+/+}$ hearts, but not from *Casz1*$^{\beta geo/\beta geo}$ hearts (Fig. 11*A*, *middle panel*). Interestingly, the E14.5 *Casz1*$^{\beta geo/\beta geo}$ cardiomyocytes, which lack a clear striated pattern, exhibit a different pattern of α-actinin staining (Fig. 11*C*). It is possible that the loss of *Casz1* delayed cardiomyocyte development or maturation, so we investigated late stage embryos and found that the disrupted striated pattern for α-actinin labeling was also observed in E15.5 *Casz1*$^{\beta geo/\beta geo}$ cardiomyocytes (data not shown). Because the embryonic lethality of *Casz1*$^{\beta geo/\beta geo}$ mice, we were not able to evaluate sarcomere formation at later developmental stages. Nevertheless, our finding that the loss of *Casz1* contributes to a disorganized sarcomeric organization in the cardiomyocytes is consistent with the GSEA assay, which indicated that loss of *Casz1* led to a negative enrichment of contractile fiber (part) gene. This indicates that *Casz1* depletion in mice results in delayed development of cardiac myocytes.

DISCUSSION

In this study, we find that *Casz1* is critical for murine heart development. Although *Casz1* has been shown to be important in heart development in *Xenopus* (17), our study indicates that loss of *Casz1* in murine hearts has a different functional impact than was shown in *Xenopus*. In this study, we demonstrated that *Casz1* deletion in mice leads to abnormal heart development including abnormal gene expression, hypoplasia of myocardium, a ventricular septal defect, and aberrant heart morphology.

Casz1 deletion also led to the embryonic lethality occurred at E17.5. Although heart failure may lead to this embryonic lethality, we cannot rule out the possibility that aberrant development of other organ such as the nervous system may be involved, because *Casz1* is highly expressed in the nervous system during embryogenesis (Fig. 1, *C* and *D*). Future studies will focus on how loss of *Casz1* affects nervous system development and embryonic lethality.

Casz1 deficiency in the murine embryonic heart led to hypoplasia of the left and right ventricles, as well as the septum, and was associated with decreased cell proliferation (Figs. 3 and 5). This contrasts with the finding that knockdown of *Casz1* in *Xenopus* heart led to overproliferation of ventral midline cells (17). One possibility that may account for the different phenotypes in these two species is that in the *Xenopus* knockdown utilized a morpholino technique, which may not be as fully penetrant as the

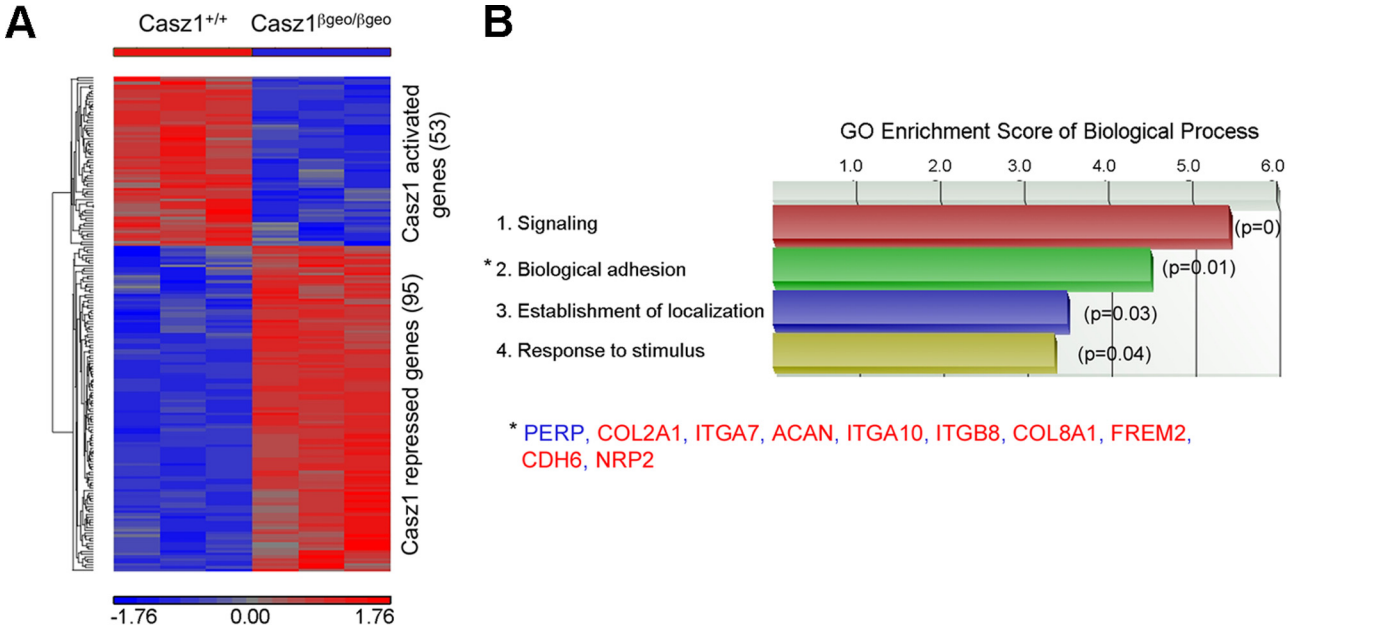

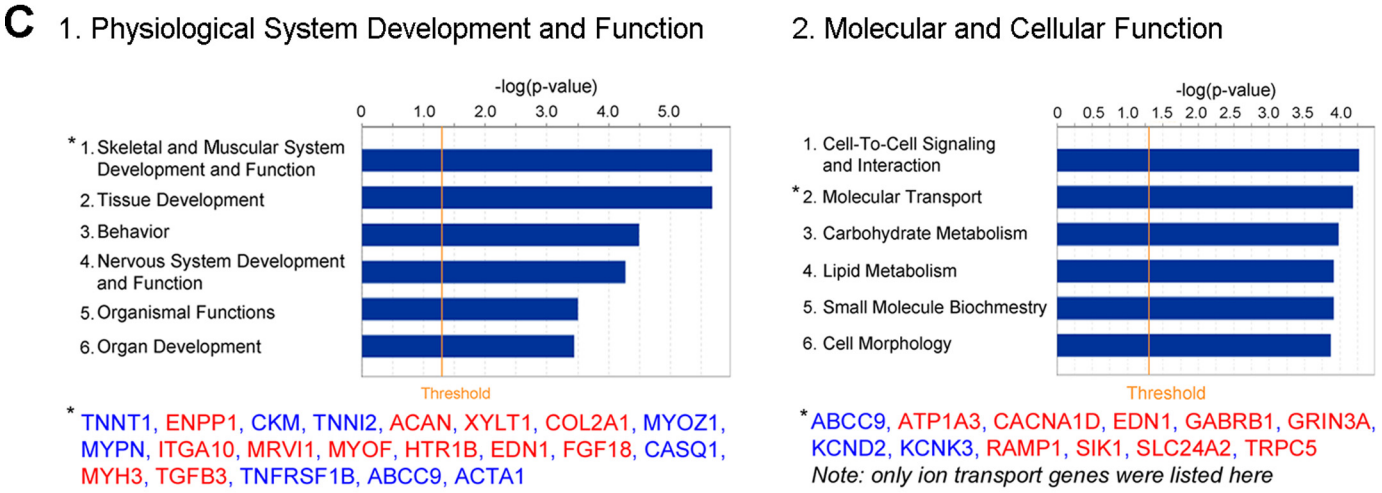

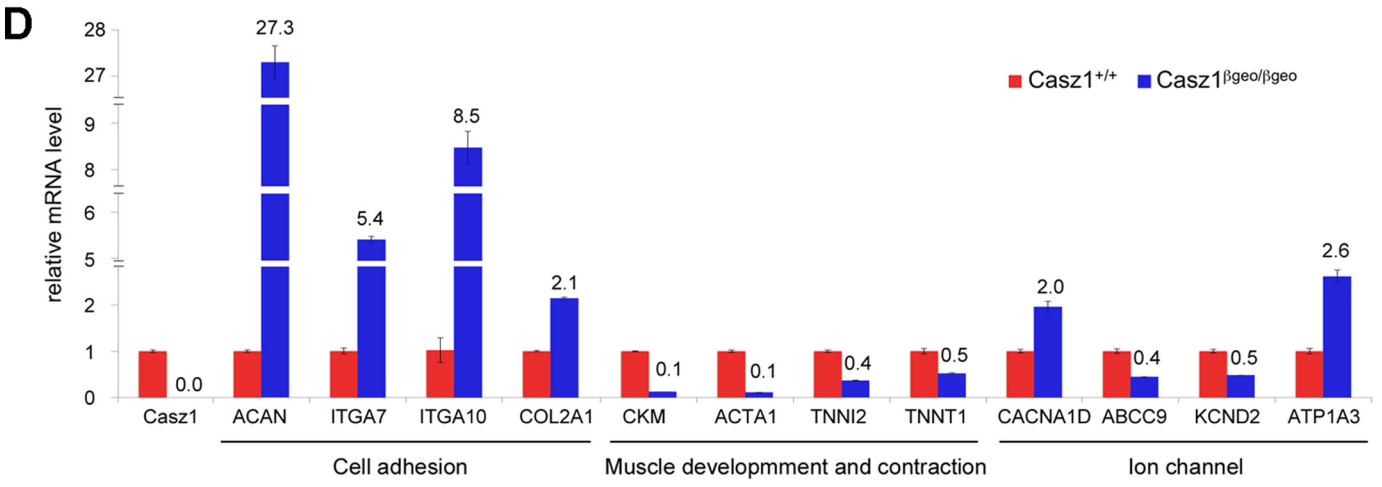

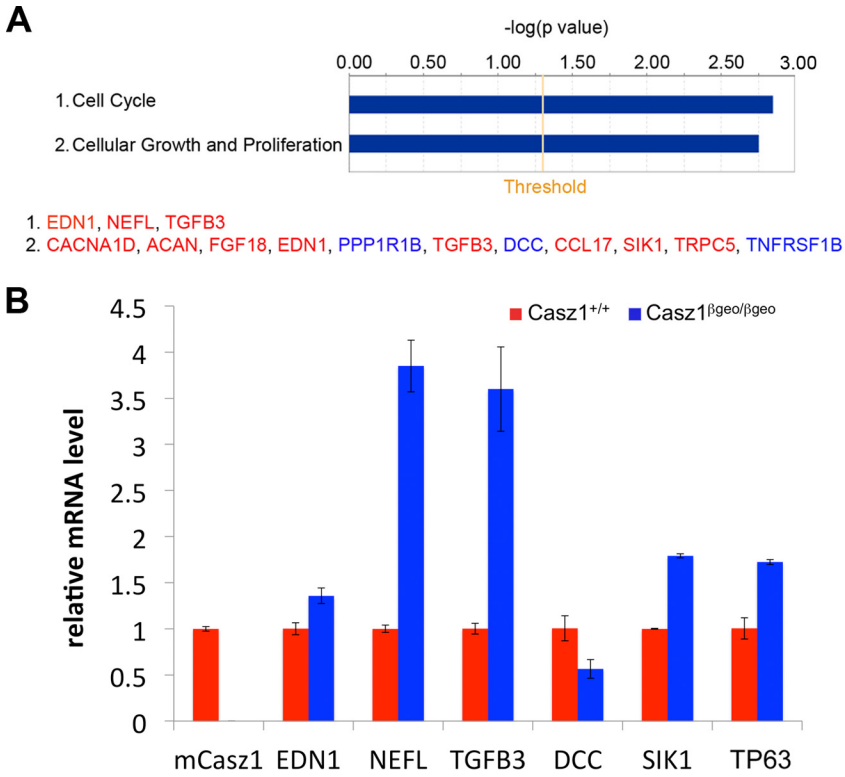

FIGURE 8. **Abnormal expression of genes involved in cell cycle and regulation of cell proliferation in *Casz1*$^{\beta geo/\beta geo}$ heart.** *A*, IPA assays showed gene enrichment in the categories of cell cycle and cellular growth and proliferation. The genes that are up-regulated (*red*) or down-regulated (*blue*) in *Casz1*$^{\beta geo/\beta geo}$ hearts were listed below. *B*, verification of microarray results. The mRNA levels of representative genes were evaluated by real time PCR and normalized to *GAPDH* gene. The mRNA levels of these genes in *Casz1*$^{\beta geo/\beta geo}$ hearts were significantly different compared with their levels in *Casz1*$^{+/+}$ hearts. The *bar graph* represents means ± S.D. (all $p < 0.05$).

Casz1- gene trapped murine model. However, it is also possible that the differences in the heart development defects noted between *Xenopus* and mice are due to the major differences in the *Casz1* gene in these species. In *Xenopus*, the *Casz1* gene encodes two isoforms Cstα (1108 amino acids) and Cstβ (1087 amino acids), and both have five zinc fingers (17). However, the murine *Casz1* locus, like the human, encodes two major isoforms; the short isoform Casz1b is similar to *Xenopus* Casz1, but the full-length isoform Casz1a has 1762 amino acids with 11 zinc fingers (12). The evolutionarily acquired six extra zinc fingers in mouse Casz1a may play certain roles during heart development through differential DNA binding or protein-protein interactions. Consistent with this hypothesis, microarray analysis of neuroblastoma cells transfected with either CASZ1a or CASZ1b showed that 16% genes were specifically regulated by either Casz1a or Casz1b (data not shown), indicating that there are some isoform-specific targets, at least in some cell types.

The murine *Casz1*-deficient hearts exhibit morphology anomalies, a ventricular septal defect and hypoplasia of myocardium (Figs. 3 and 5), which may be caused by abnormal gene expression. Cardiac morphogenesis is a complex process that is coordinately regulated by many transcription factors such as *Nkx2-5*, *TBX5*, *GATA4*, and *GATA6* (3–5, 7). Casz1 is a novel transcription factor highly expressed in heart, and we found that abnormal expression of cell adhesion genes are significantly enriched in *Casz1*-deficient heart (Fig. 7*B*). Cell adhesion molecules play critical role for embryo and tissue morphogenesis (29, 30). *Casz1* regulates cadherin family protein (*CDH6*), collagens (*COL2A1* and *COL8A1*), and integrins (*ITGA7*, *ITGA10*, and *ITGB8*), which are known to be important for tissue morphogenesis (31–33). Although it has not been reported that these genes specifically affect cardiac morphogenesis, the abnormal expression of such cell adhesion genes may contribute to the disorganized morphology in *Casz1*$^{\beta geo/\beta geo}$ heart. The dysregulation of genes involved in cell cycle and cell growth regulation in *Casz1*-deficient heart (Fig. 8) may lead to hypoplasia of myocardium. For example, both *TGFB3* and *TP63* are able to induce cell cycle arrest and inhibit cell proliferation (34–37), so the up-regulation of these genes in *Casz1*-deficient heart may lead to the decrease of cardiomyocyte proliferation.

FIGURE 7. **Abnormal gene expression in *Casz1*$^{\beta geo/\beta geo}$ heart.** *A*, microarray analysis of RNA from three E12.5 *Casz1*$^{+/+}$ hearts and three E12.5 *Casz1*$^{\beta geo/\beta geo}$ hearts. The heat map was generated using Partek software. Two-thirds of these genes are aberrantly up-regulated, and one-third are aberrantly down regulated in *Casz1*$^{\beta geo/\beta geo}$ hearts. *B*, Partek gene ontology oncology analysis showed that the top two categories of enriched genes are "signaling" and the process of biological adhesion. Biological adhesion genes in *Casz1*$^{\beta geo/\beta geo}$ hearts that are up-regulated (*red*) or down-regulated (*blue*) are listed below. *C*, IPA assays showed gene enrichment in the categories of physiological system development and function (*panel 1*) with a key subcategory being skeletal and muscular system development and function genes that are up-regulated (*red*) or down-regulated (*blue*) in *Casz1*$^{\beta geo/\beta geo}$ hearts listed below and molecular and cellular function (*panel 2*) with a key subcategory of genes in molecular transport and the ion transport genes that are up-regulated (*red*) or down-regulated (*blue*) listed below. *D*, verification of microarray results. The mRNA levels of representative genes encoding cell adhesion molecules, muscle contraction, and muscular development proteins and ion channels were evaluated by real time PCR and normalized to *GAPDH* gene. The mRNA levels of these genes in *Casz1*$^{\beta geo/\beta geo}$ hearts were significantly different compared with their levels in *Casz1*$^{+/+}$ hearts. The *bar graph* represents means ± S.D. (all $p < 0.005$).

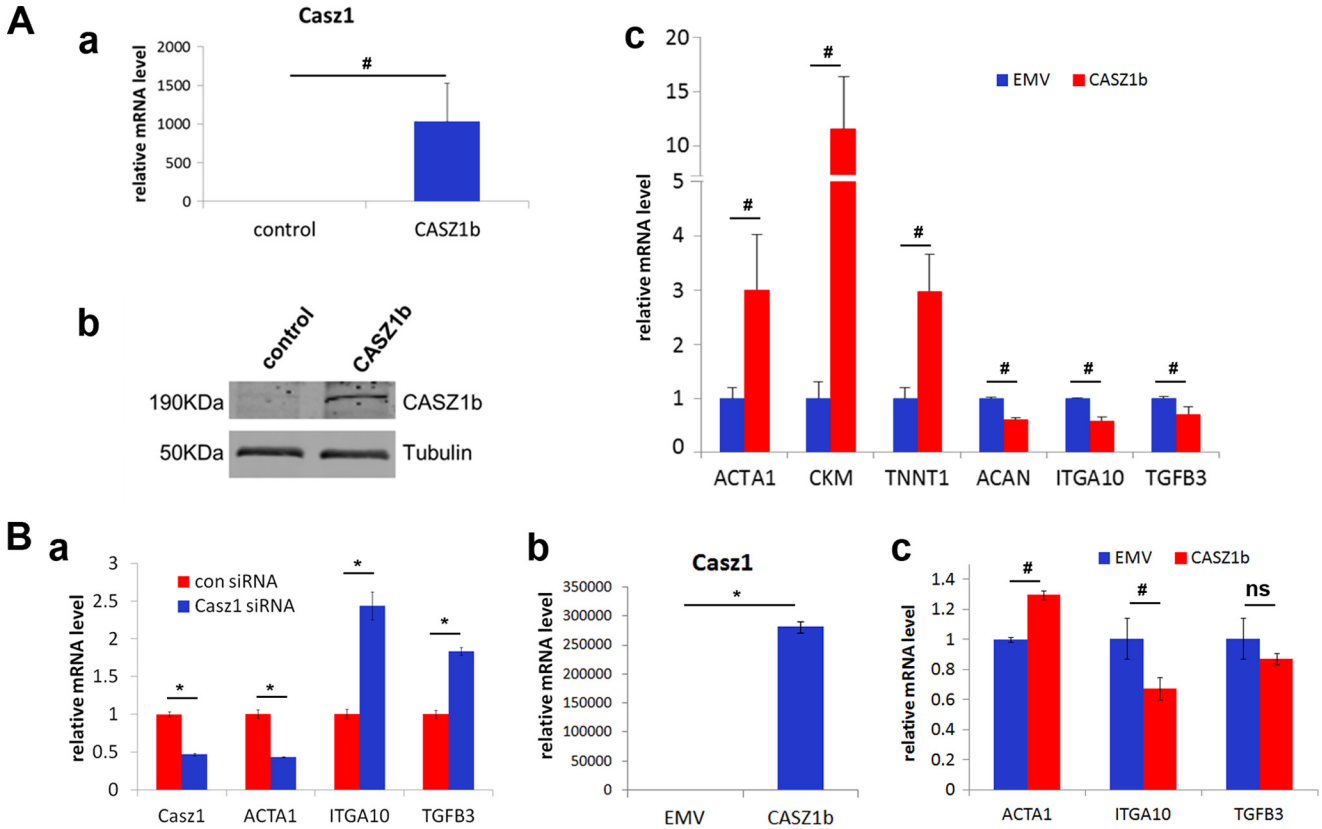

FIGURE 9. **Validation of Casz1 target genes in cellular models.** *A*, human cardiac fibroblasts were transfected with empty vector (*EMV*) or CASZ1b vector and cultured for 5 days. *Panel a*, relative CASZ1b mRNA level was evaluated by real time PCR using human *CASZ1* primer. The *bar graph* represents means ± S.E.(#, $p < 0.05$). *Panel b*, Western blot to show the overexpression of *Casz1b* in CASZ1b overexpressed cells. *Panel c*, after overexpression of CASZ1b, relative mRNA levels of representative genes were evaluated by real time PCR. The *bar graph* represents means ± S.E. (#, $p < 0.05$). *B*, knockdown or overexpression of *Casz1* in HL-1 cells. *Panel a*, HL-1 cells were transfected with nontargeting control (*con*) siRNA or *Casz1* siRNA, and after a 2-day culture, the relative mRNA levels of representative genes were evaluated by real time. The *bar graph* represents means ± S.D. (*, $p < 0.005$). *Panel b*, HL-1 cells were transfected with EMV or CASZ1b vector, and after a 2-day culture, the relative CASZ1b mRNA levels were evaluated by real time PCR using human *CASZ1* primers. The *graph* represents mean ± S.D. (*, $p < 0.005$). *Panel c*, after transfection with CASZ1b and a two-dimensional culture, the relative mRNA levels of representative genes were evaluated by real time PCR. The *bar graph* represents means ± S.D. (#, $p < 0.05$; *ns* represents no statistic significant difference).

The abnormal expression of muscle development and function genes, as well as the genes encoding contractile filament proteins in the *Casz1*$^{\beta geo/\beta geo}$ heart (Figs. 7 and 10*A*), may contribute to the heart abnormalities. Among muscle development and function genes, *CASQ1*, *TNNT1*, and *TNNI2* are genes required for muscle contraction (38–41). Gene ontology assay using GSEA tool showed that 50% of the contractile fiber genes were negatively enriched in *Casz1* mutant heart (Fig. 10*A*), although among most of them, their expression level only decreased 10–20%, but as a group, the combined decrease can lead to a significant phenotype and biofunction change. Among these contractile fiber genes, the *ACTA1* level decreased 90% in *Casz1* mutant heart. As a contractile fiber gene, ACTA1 is important for the organization of the sarcomeres (39). Consistent with the finding of dysregulation of contractile fiber gene expression, we found that *Casz1*-deficient cardiomyocytes displayed abnormal Z line formation (Fig. 11). Because cardiac Z line plays an important role in cardiomyocyte signal transduction and disease and sarcomeres play a critical role in cardiac pump functions (39, 42–45), it suggests dysregulation of contractile fiber genes and muscle contraction genes in *Casz1*-deficient heart contributes to the heart failure.

The cause of heart defects in *Casz1* deletion embryos is likely due to altered expression of multiple *Casz1* downstream targets acting in combination, because many *Casz1* target genes are reported to be important for heart function and/or have been implicated in CHD. For example, a mutation in the muscle contraction gene *ACTA1* was found in a case of nonfatal hypertrophic cardiomyopathy (46), and *TNNI2* mutations were found in hypertrophic cardiomyopathy (47); mutations in developmental gene *TGFB3* were found in right ventricular cardiomyopathy disease (48, 49). Ion channels such as potassium channels and calcium channels are important for cardiac conduction (50–53), and they were transcriptionally regulated by key cardiac transcriptional factors (54). Mutations in *ABCC9* a potassium channel gene were identified in human dilated cardiomyopathy (55). The involvement of many of these genes in heart function raises the possibility that these genes work in combination to mediate *Casz1* regulatory functions during heart development.

In fact, key cardiac transcription factors control heart development via regulation of sets of genes that mediate cardiac morphogenesis and contractility (3–6). *Casz1* targets overlap with targets of known cardiac transcription factors such as *MYOCD*, *MEF2C*, and *GATA4*. For example, *ACTA1*, *CACNA1D*, *COL2A1*, *TAGLN*, and *LMOD1* are regulated by *Casz1*, as well as *MYOCD*. *ACTA1*, *CKM*, *MYOZ1*, and *COL2A1* are regulated by *Casz1*, as well as *MEF2C*. Although

A a

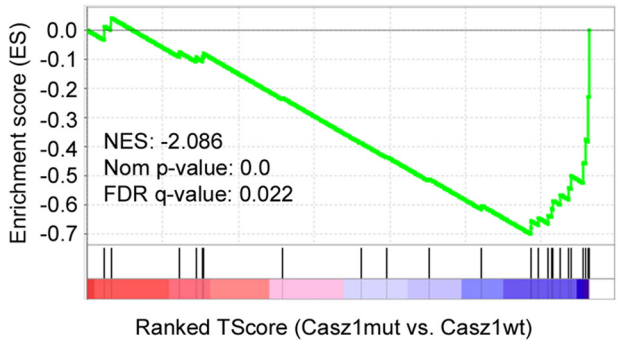

b Contractile fiber gene details in GSEA

	PROBE	RANK IN GENE LIST	RANK METRIC SCORE	RUNNING ES	CORE ENRICHMENT
1	ABRA	591	3.658	0.0127	No
2	MYL6B	796	3.209	0.0429	No
3	TPM3	3050	1.329	-0.0756	No
4	VCL	3599	1.128	-0.0938	No
5	TPM2	3822	1.052	-0.0933	No
6	DES	3843	1.042	-0.0807	No
7	CDK5R1	6459	0.404	-0.2333	No
8	TNNI3	9041	-0.110	-0.3878	No
9	TPM4	9913	-0.283	-0.4367	No
10	TNNT2	11283	-0.577	-0.5117	No
11	MYBPC1	13025	-1.028	-0.6033	No
12	KRT19	14646	-1.714	-0.6785	Yes
13	SVIL	14676	-1.734	-0.6573	Yes
14	DMD	14913	-1.874	-0.6467	Yes
15	MYL3	15232	-2.132	-0.6377	Yes
16	MYL9	15333	-2.241	-0.6140	Yes
17	NEB	15395	-2.310	-0.5871	Yes
18	TTN	15632	-2.641	-0.5664	Yes
19	MYOZ2	15909	-3.128	-0.5417	Yes
20	TNNC1	15987	-3.342	-0.5021	Yes
21	MYLPF	16397	-5.257	-0.4572	Yes
22	TPM1	16466	-6.355	-0.3771	Yes
23	MYOM1	16558	-11.604	-0.2290	Yes
24	ACTA1	16570	-17.363	0.0003	Yes

c

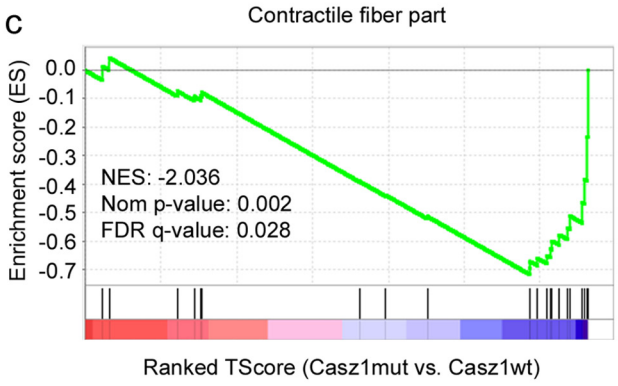

B

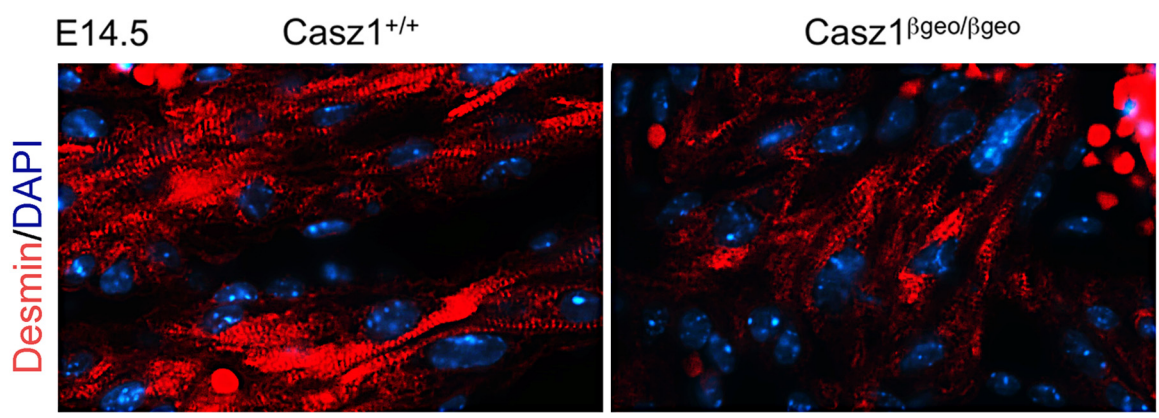

FIGURE 10. **Sarcomeric organization in *Casz1*$^{\beta geo/\beta geo}$ heart.** *A*, GSEA assay indicated the negative enrichment of genes encoding contractile fiber proteins (*panels a* and *b*), as well as genes encoding contractile fiber part proteins (*panel c*). *NES,* normalized enrichment score; *Nom,* nominal; *FDR,* false discovery rate. *B*, sections containing the trabecular regions of E14.5 hearts were labeled for desmin (*red*), and nuclei were stained with DAPI (*blue*). There is a striated pattern for desmin labeling in both wild type and *Casz1*-deficient hearts, but the striated patterns are not as uniform or apparent in the *Casz1*-deficient heart.

these genes are both regulated by *Casz1* and *MYOCD* or *MEF2C*, they were not regulated in the same direction (up or down), which suggests that *Casz1* is not downstream or upstream of *MYOCD* or *MEF2C*. *Casz1* may cooperate with them to ensure that these genes are expressed at the appropriate level or time during heart development. It is unclear at present whether these genes are direct targets of *Casz1* because of a lack of a ChIP grade Casz1 antibody, but our future plan will include the identification of *Casz1* direct targets in heart. Nevertheless, using two different *in vitro* cellular models, we confirmed that many of the muscle development genes, contract fiber genes, and cell adhesion genes regulated by loss of *Casz1* in the heart *in vivo* were similarly regulated by *Casz1* in these cellular models *in vitro* (Fig. 9).

Our finding that *Casz1* is critical for mammalian heart development and *Casz1* target genes are related to the pathogenesis of CHD suggests that *Casz1* may be a novel CHD gene. *Casz1* homozygous deletion in mice led to heart failure and embryonic lethality, although the *Casz1* heterozygous deletion did not show apparent abnormalities in mice. This is not unusual because some CHD causative genes cause severe heart defect and embryonic lethality in the homozygous gene knock-outs,

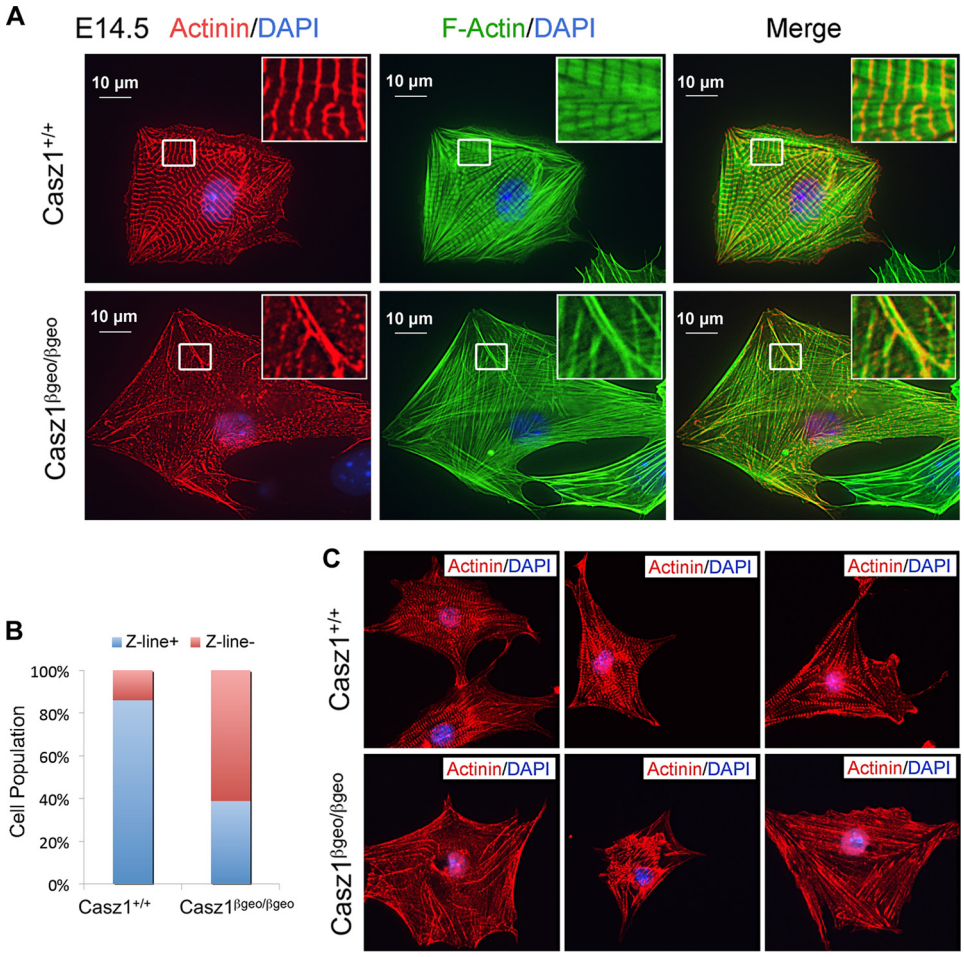

FIGURE 11. **Abnormal Z line organization in E14.5 *Casz1*$^{\beta geo/\beta geo}$ heart.** *A*, cardiomyocytes isolated from *Casz1*$^{+/+}$ and *Casz1*$^{\beta geo/\beta geo}$ E14.5 embryo hearts were cultured *in vitro* for 2 days and immunostained for α-actinin (*red*) and F-actin (*green*), whereas the nuclei were stained with DAPI (*blue*). Representative images show that clear Z lines were presented in the wild type cardiomyocytes, but not in the *Casz1*$^{\beta geo/\beta geo}$ cardiomyocytes. *B*, the CHITEST histogram shows the percentage of *Casz1*$^{+/+}$ or *Casz1*$^{\beta geo/\beta geo}$ cardiomyocytes with clear Z lines (*Z line*+) or abnormal Z lines (*Z line*−) ($p < 0.00001$). The data are from two independent experiments (>100 *Casz1*$^{+/+}$ or *Casz1*$^{\beta geo/\beta geo}$ cardiomyocytes were counted in each experiment). *C*, more representative images show that clear Z lines are present in the *Casz1*$^{+/+}$ cardiomyocytes. There are no clear Z lines in these *Casz1*$^{\beta geo/\beta geo}$ cardiomyocytes, and the α-actinin staining pattern is distinct compared with the *Casz1*$^{+/+}$ cardiomyocytes.

but no apparent heart anomalies in heterozygous mice (56–58). *CASZ1* resides on chromosome 1p36.22. Chr1p36 deletion is one of the most common terminal deletions observed in humans, and monosomy 1p36 is associated with many diseases such as central nervous system malformations (88%), skeletal anomalies, and heart defects (71–75%), but the 1p36 genes that contribute to heart disease have not been clearly delineated (2, 16, 59). Interestingly, 1p36 deletion-related CHD includes cardiac noncompaction and ventricular septal defect (2, 16), which was also seen in our *Casz1*-deficient heart (Figs. 3 and 5). Although no mutations of *CASZ1* have been reported in CHD patients, loss of heterozygosity of *CASZ1* occurs in those patients with 1p36 deletion syndrome-related CHD. Recent exome sequencing results discovered *de novo* mutations in histone-modifying genes in CHD that contribute to ~10% of severe CHD, in which the key developmental genes expression were dysregulated (60). We have shown that one allele of *CASZ1* may be lost by 1p36LOH in neuroblastoma tumors, and the other allele may be epigenetically silenced by PRC2 complex-mediated histone modifications (61). This raises the possibility that *CASZ1* expression may be dysregulated in CHD with *de novo* mutations in histone modifying genes. Importantly, our previous study has shown that HDAC inhibitor treatment of neuroblastoma cells leads to an increase of *CASZ1* expression (61), suggesting a potential therapeutic modality.

Our data clearly demonstrate that *CASZ1* is a novel cardiac transcription factor that plays an important role in cardiac development and morphogenesis in mammals. *CASZ1* is a candidate CHD associated gene, and genetic or epigenetic alteration on the *CASZ1* gene may contribute to CHD.

Acknowledgments—We thank Dr. Robert S. Adelstein for thoughtful review and comments on this project; Dr. Simone Difilippantonio, Mary Albaugh, Cari Graff-Cherry, Jennifer Waters, and Juanita Mercado (NCI-Frederick Animal Core Facility) for taking care of the Casz1-trapped mice; Dr. Xiaolin Wu from Laboratory of Molecular Technology of NCI-Frederic for microarray services; Drs. Ulrich Baxa and Kunio Nagashima (Electron Microscope Laboratory of NCI-Frederick) for electron microscope service; Drs. Amber Giles, Meera Murgai, and Rosandra Kaplan for kind assistance and advice with the Zeiss ApoTome microscopy images; and Bill Nguyen and Richard Wang for help with the mice genotyping.

REFERENCES

1. Hoffman, J. I., and Kaplan, S. (2002) The incidence of congenital heart disease. *J. Am. Coll. Cardiol.* **39,** 1890–1900
2. Fahed, A. C., Gelb, B. D., Seidman, J. G., and Seidman, C. E. (2013) Genetics of congenital heart disease: the glass half empty. *Circ. Res.* **112,** 707–720
3. Bruneau, B. G. (2013) Signaling and transcriptional networks in heart development and regeneration. *Cold Spring Harb. Perspect. Biol.* **5,** a008292
4. Srivastava, D. (2006) Making or breaking the heart: from lineage determination to morphogenesis. *Cell* **126,** 1037–1048
5. Olson, E. N. (2006) Gene regulatory networks in the evolution and development of the heart. *Science* **313,** 1922–1927
6. Srivastava, D., and Olson, E. N. (2000) A genetic blueprint for cardiac development. *Nature* **407,** 221–226
7. McCulley, D. J., and Black, B. L. (2012) Transcription factor pathways and congenital heart disease. *Curr. Top. Dev. Biol.* **100,** 253–277
8. Cui, X., and Doe, C. Q. (1992) ming is expressed in neuroblast sublineages and regulates gene expression in the *Drosophila* central nervous system. *Development* **116,** 943–952
9. Mellerick, D. M., Kassis, J. A., Zhang, S. D., and Odenwald, W. F. (1992) Castor encodes a novel zinc finger protein required for the development of a subset of CNS neurons in *Drosophila*. *Neuron* **9,** 789–803
10. Vacalla, C. M., and Theil, T. (2002) Cst, a novel mouse gene related to *Drosophila* Castor, exhibits dynamic expression patterns during neurogenesis and heart development. *Mech. Dev.* **118,** 265–268
11. Liu, Z., Yang, X., Tan, F., Cullion, K., and Thiele, C. J. (2006) Molecular cloning and characterization of human Castor, a novel human gene upregulated during cell differentiation. *Biochem. Biophys. Res. Commun.* **344,** 834–844
12. Liu, Z., Naranjo, A., and Thiele, C. J. (2011) CASZ1b, the short isoform of CASZ1 gene, coexpresses with CASZ1a during neurogenesis and suppresses neuroblastoma cell growth. *PLoS One* **6,** e18557
13. Liu, Z., Yang, X., Li, Z., McMahon, C., Sizer, C., Barenboim-Stapleton, L., Bliskovsky, V., Mock, B., Ried, T., London, W. B., Maris, J., Khan, J., and Thiele, C. J. (2011) CASZ1, a candidate tumor-suppressor gene, suppresses neuroblastoma tumor growth through reprogramming gene expression. *Cell Death Differ.* **18,** 1174–1183
14. Virden, R. A., Thiele, C. J., and Liu, Z. (2012) Characterization of critical domains within the tumor suppressor CASZ1 required for transcriptional regulation and growth suppression. *Mol. Cell. Biol.* **32,** 1518–1528
15. Henrich, K. O., Schwab, M., and Westermann, F. (2012) 1p36 tumor suppression: a matter of dosage? *Cancer Res.* **72,** 6079–6088
16. Gajecka, M., Mackay, K. L., and Shaffer, L. G. (2007) Monosomy 1p36 deletion syndrome. *Am. J. Med. Genet. C Semin. Med. Genet.* **145C,** 346–356
17. Christine, K. S., and Conlon, F. L. (2008) Vertebrate CASTOR is required for differentiation of cardiac precursor cells at the ventral midline. *Dev. Cell* **14,** 616–623
18. Charpentier, M. S., Christine, K. S., Amin, N. M., Dorr, K. M., Kushner, E. J., Bautch, V. L., Taylor, J. M., and Conlon, F. L. (2013) CASZ1 promotes vascular assembly and morphogenesis through the direct regulation of an EGFL7/RhoA-mediated pathway. *Dev. Cell* **25,** 132–143
19. Reid, S. W., and Tessarollo, L. (2009) Isolation, microinjection and transfer of mouse blastocysts. *Methods Mol. Biol.* **530,** 269–285
20. Gerety, S. S., and Anderson, D. J. (2002) Cardiovascular ephrinB2 function is essential for embryonic angiogenesis. *Development* **129,** 1397–1410
21. Vecellio, M., Spallotta, F., Nanni, S., Colussi, C., Cencioni, C., Derlet, A., Bassetti, B., Tilenni, M., Carena, M. C., Farsetti, A., Sbardella, G., Castellano, S., Mai, A., Martelli, F., Pompilio, G., Capogrossi, M. C., Rossini, A., Dimmeler, S., Zeiher, A., and Gaetano, C. (2014) The histone acetylase activator pentadecylidenemalonate 1b rescues proliferation and differentiation in the human cardiac mesenchymal cells of type 2 diabetic patients. *Diabetes* **63,** 2132–2147
22. Rossini, A., Frati, C., Lagrasta, C., Graiani, G., Scopece, A., Cavalli, S., Musso, E., Baccarin, M., Di Segni, M., Fagnoni, F., Germani, A., Quaini, E., Mayr, M., Xu, Q., Barbuti, A., DiFrancesco, D., Pompilio, G., Quaini, F., Gaetano, C., and Capogrossi, M. C. (2011) Human cardiac and bone marrow stromal cells exhibit distinctive properties related to their origin. *Cardiovasc. Res.* **89,** 650–660
23. Claycomb, W. C., Lanson, N. A., Jr., Stallworth, B. S., Egeland, D. B., Delcarpio, J. B., Bahinski, A., and Izzo, N. J., Jr. (1998) HL-1 cells: a cardiac muscle cell line that contracts and retains phenotypic characteristics of the adult cardiomyocyte. *Proc. Natl. Acad. Sci. U.S.A.* **95,** 2979–2984
24. Greenberg, C. C., Connelly, P. S., Daniels, M. P., and Horowits, R. (2008) Krp1 (Sarcosin) promotes lateral fusion of myofibril assembly intermediates in cultured mouse cardiomyocytes. *Exp. Cell Res.* **314,** 1177–1191
25. Ma, X., Jana, S. S., Conti, M. A., Kawamoto, S., Claycomb, W. C., and Adelstein, R. S. (2010) Ablation of nonmuscle myosin II-B and II-C reveals a role for nonmuscle myosin II in cardiac myocyte karyokinesis. *Mol. Biol. Cell* **21,** 3952–3962
26. Li, W., Kohara, H., Uchida, Y., James, J. M., Soneji, K., Cronshaw, D. G., Zou, Y. R., Nagasawa, T., and Mukouyama, Y. S. (2013) Peripheral nerve-derived CXCL12 and VEGF-A regulate the patterning of arterial vessel branching in developing limb skin. *Dev. Cell* **24,** 359–371
27. Li, W., and Mukouyama, Y. S. (2011) Whole-mount immunohistochemical analysis for embryonic limb skin vasculature: a model system to study vascular branching morphogenesis in embryo. *J. Vis. Exp.* **pii,** 2620
28. Spallotta, F., Cencioni, C., Straino, S., Nanni, S., Rosati, J., Artuso, S., Manni, I., Colussi, C., Piaggio, G., Martelli, F., Valente, S., Mai, A., Capogrossi, M. C., Farsetti, A., and Gaetano, C. (2013) A nitric oxide-dependent cross-talk between class I and III histone deacetylases accelerates skin repair. *J. Biol. Chem.* **288,** 11004–11012
29. Barone, V., and Heisenberg, C. P. (2012) Cell adhesion in embryo morphogenesis. *Curr. Opin. Cell Biol.* **24,** 148–153
30. Lecuit, T., and Lenne, P. F. (2007) Cell surface mechanics and the control of cell shape, tissue patterns and morphogenesis. *Nat. Rev. Mol. Cell Biol.* **8,** 633–644
31. Larsen, M., Artym, V. V., Green, J. A., and Yamada, K. M. (2006) The matrix reorganized: extracellular matrix remodeling and integrin signaling. *Curr. Opin. Cell Biol.* **18,** 463–471
32. Corda, S., Samuel, J. L., and Rappaport, L. (2000) Extracellular matrix and growth factors during heart growth. *Heart Fail Rev.* **5,** 119–130
33. Gumbiner, B. M. (2005) Regulation of cadherin-mediated adhesion in morphogenesis. *Nat. Rev. Mol. Cell Biol.* **6,** 622–634
34. Nakamura, S., Kawai, T., Kamakura, T., and Ookura, T. (2010) TGF-β3 is expressed in taste buds and inhibits proliferation of primary cultured taste epithelial cells. *In Vitro Cell. Dev. Biol. Anim.* **46,** 36–44
35. Iordanskaia, T., and Nawshad, A. (2011) Mechanisms of transforming growth factor β induced cell cycle arrest in palate development. *J. Cell. Physiol.* **226,** 1415–1424
36. Little, N. A., and Jochemsen, A. G. (2002) p63. *Int. J. Biochem. Cell Biol.* **34,** 6–9
37. Allocati, N., Di Ilio, C., and De Laurenzi, V. (2012) p63/p73 in the control of cell cycle and cell death. *Exp. Cell Res.* **318,** 1285–1290
38. Mosca, B., Delbono, O., Laura Messi, M., Bergamelli, L., Wang, Z. M., Vukcevic, M., Lopez, R., Treves, S., Nishi, M., Takeshima, H., Paolini, C., Martini, M., Rispoli, G., Protasi, F., and Zorzato, F. (2013) Enhanced dihydropyridine receptor calcium channel activity restores muscle strength in JP45/CASQ1 double knockout mice. *Nat. Commun.* **4,** 1541
39. Clarkson, E., Costa, C. F., and Machesky, L. M. (2004) Congenital myopathies: diseases of the actin cytoskeleton. *J. Pathol.* **204,** 407–417
40. Robaszkiewicz, K., and Moraczewska, J. (2011) [Congenital myopathies: skeletal muscle diseases related to disorder of actin filament structure and functions]. *Postepy. Hig. Med. Dosw.* (*Online*) **65,** 347–356
41. Kimber, E., Tajsharghi, H., Kroksmark, A. K., Oldfors, A., and Tulinius, M. (2006) A mutation in the fast skeletal muscle troponin I gene causes myopathy and distal arthrogryposis. *Neurology* **67,** 597–601
42. Hein, S., Kostin, S., Heling, A., Maeno, Y., and Schaper, J. (2000) The role of the cytoskeleton in heart failure. *Cardiovasc. Res.* **45,** 273–278
43. Chang, A. N., and Potter, J. D. (2005) Sarcomeric protein mutations in dilated cardiomyopathy. *Heart Fail. Rev.* **10,** 225–235
44. Solaro, R. J., and de Tombe, P. P. (2008) Review focus series: sarcomeric proteins as key elements in integrated control of cardiac function. *Cardiovasc. Res.* **77,** 616–618

45. Frank, D., and Frey, N. (2011) Cardiac Z-disc signaling network. *J. Biol. Chem.* **286,** 9897–9904
46. Kim, S. Y., Park, Y. E., Kim, H. S., Lee, C. H., Yang, D. H., and Kim, D. S. (2011) Nemaline myopathy and non-fatal hypertrophic cardiomyopathy caused by a novel ACTA1 E239K mutation. *J. Neurol. Sci.* **307,** 171–173
47. Tsoutsman, T., Bagnall, R. D., and Semsarian, C. (2008) Impact of multiple gene mutations in determining the severity of cardiomyopathy and heart failure. *Clin. Exp. Pharmacol. Physiol.* **35,** 1349–1357
48. Lombardi, R., and Marian, A. J. (2011) Molecular genetics and pathogenesis of arrhythmogenic right ventricular cardiomyopathy: a disease of cardiac stem cells. *Pediatr. Cardiol.* **32,** 360–365
49. Beffagna, G., Occhi, G., Nava, A., Vitiello, L., Ditadi, A., Basso, C., Bauce, B., Carraro, G., Thiene, G., Towbin, J. A., Danieli, G. A., and Rampazzo, A. (2005) Regulatory mutations in transforming growth factor-β3 gene cause arrhythmogenic right ventricular cardiomyopathy type 1. *Cardiovasc. Res.* **65,** 366–373
50. Nichols, C. G., Singh, G. K., and Grange, D. K. (2013) KATP channels and cardiovascular disease: suddenly a syndrome. *Circ. Res.* **112,** 1059–1072
51. Giudicessi, J. R., and Ackerman, M. J. (2012) Potassium-channel mutations and cardiac arrhythmias: diagnosis and therapy. *Nat. Rev. Cardiol.* **9,** 319–332
52. Cerrone, M., Napolitano, C., and Priori, S. G. (2012) Genetics of ion-channel disorders. *Curr. Opin. Cardiol.* **27,** 242–252
53. Venetucci, L., Denegri, M., Napolitano, C., and Priori, S. G. (2012) Inherited calcium channelopathies in the pathophysiology of arrhythmias. *Nat. Rev. Cardiol.* **9,** 561–575
54. Hatcher, C. J., and Basson, C. T. (2009) Specification of the cardiac conduction system by transcription factors. *Circ. Res.* **105,** 620–630
55. Bienengraeber, M., Olson, T. M., Selivanov, V. A., Kathmann, E. C., O'Cochlain, F., Gao, F., Karger, A. B., Ballew, J. D., Hodgson, D. M., Zingman, L. V., Pang, Y. P., Alekseev, A. E., and Terzic, A. (2004) ABCC9 mutations identified in human dilated cardiomyopathy disrupt catalytic KATP channel gating. *Nat. Genet.* **36,** 382–387
56. Maitra, M., Schluterman, M. K., Nichols, H. A., Richardson, J. A., Lo, C. W., Srivastava, D., and Garg, V. (2009) Interaction of Gata4 and Gata6 with Tbx5 is critical for normal cardiac development. *Dev. Biol.* **326,** 368–377
57. Stennard, F. A., and Harvey, R. P. (2005) T-box transcription factors and their roles in regulatory hierarchies in the developing heart. *Development* **132,** 4897–4910
58. Molkentin, J. D., Lin, Q., Duncan, S. A., and Olson, E. N. (1997) Requirement of the transcription factor GATA4 for heart tube formation and ventral morphogenesis. *Genes Dev.* **11,** 1061–1072
59. Zhu, X., Zhang, Y., Wang, J., Yang, J. F., Yang, Y. F., and Tan, Z. P. (2013) 576 kb deletion in 1p36.33-p36.32 containing SKI is associated with limb malformation, congenital heart disease and epilepsy. *Gene* **528,** 352–355
60. Zaidi, S., Choi, M., Wakimoto, H., Ma, L., Jiang, J., Overton, J. D., Romano-Adesman, A., Bjornson, R. D., Breitbart, R. E., Brown, K. K., Carriero, N. J., Cheung, Y. H., Deanfield, J., DePalma, S., Fakhro, K. A., Glessner, J., Hakonarson, H., Italia, M. J., Kaltman, J. R., Kaski, J., Kim, R., Kline, J. K., Lee, T., Leipzig, J., Lopez, A., Mane, S. M., Mitchell, L. E., Newburger, J. W., Parfenov, M., Pe'er, I., Porter, G., Roberts, A. E., Sachidanandam, R., Sanders, S. J., Seiden, H. S., State, M. W., Subramanian, S., Tikhonova, I. R., Wang, W., Warburton, D., White, P. S., Williams, I. A., Zhao, H., Seidman, J. G., Brueckner, M., Chung, W. K., Gelb, B. D., Goldmuntz, E., Seidman, C. E., and Lifton, R. P. (2013) De novo mutations in histone-modifying genes in congenital heart disease. *Nature* **498,** 220–223
61. Wang, C., Liu, Z., Woo, C. W., Li, Z., Wang, L., Wei, J. S., Marquez, V. E., Bates, S. E., Jin, Q., Khan, J., Ge, K., and Thiele, C. J. (2012) EZH2 Mediates epigenetic silencing of neuroblastoma suppressor genes CASZ1, CLU, RUNX3, and NGFR. *Cancer Res.* **72,** 315–324